Cold forging METAL forming real Scenario testing on Disc by using Finite Element Analysis

ABSTRACT

FINITE ELEMENT ANALYSIS OF FORGING

Numerical modeling and simulation of metal forming is very effective in saving production time, effort and economy and has thus gained prominence in many industries all over the world. In metal-forming finite element analysis, software like Deform, Qform, Forge, Simufact, Hyperform are used extensively for the forming analysis. Apart from having narrow applications, these software are expensive. The object of this study was to examine the robustness of general package software in regards to forging. Software such as Abaqus and Ansys LSDyna were used to simulate the forging process. The case examined was that of a circular metal disc restrained at the outer boundary and deformed from the center.

TABLE OF CONTENTS

LIST OF ILLUSTRATIONS

Chapter Page

LIST OF TABLES

Chapter Page

CHAPTER 1

INTRODUCTION

1.1 Introduction

The process of forging is concerned with the shaping of metals by the application of compressive forces. Depending on the temperature range, the process of forging is categorized into three, viz. cold forging, warm forging and hot forging.

Cold forging is carried out at or near room temperatures. Generally, impression die forging or true closed forging comes in the category of cold forging. Carbon and standard alloy steels are most commonly cold-forged.

The temperature range for the warm forging of steel is from above room temperature to below the re-crystallization temperature of the metal being forged, or from about 800 to 1,800 degrees Fahrenheit. Warm forging has the advantages of reduced tooling loads, reduced press loads and increased steel ductility as compared to cold forging.

Hot forging is carried out at temperatures above the re-crystallization temperatures of metals. This forging process leads to high ductility, since re-crystallization keeps the material from strain hardening, which keeps the yield strength and hardness low [1].

Usually, in a forging process a simple billet geometry is transformed into a required part shape by a sequence of forming operations. During the forming process, the intermediate steps and corresponding shapes required to produce the final forging are determined by the process engineer, meeting requirements such as tolerances, flash conditions, concentricities, tonnages, tool life, and so on. In recent past, the forming sequence was carried out by trial and error method or by past experience and empirical relationships leading to extensive and expensive die trials and modifications. Iterations involved the cost of tools and the downtime of the

equipment. For the optimization and reduction of costly trial iterations in the forming process an insight into the deformation mechanics could prove to be very useful [2].

Of late, metal forming software packages like DEFORM, Forge, Hyperform, Simufact, Qform, et cetera, are being used in industries for the finite element analysis of the metal forming process. The high cost and limited applications (restricted only to the metal forming operations) of these packages render them inadequate in regards to other finite element analyses and can be a bad investment for multi-solution providing industries.

This paper tests the forging ability of general package software like Ansys-LSDyna and Abaqus. "*Ansys-LSDyna is a collaboration between ANSYS Inc. and Livermore Technology Software Corporation. Driven by Livermore Technology Software Corporation's explicit dynamic solver technology and the pre and post-processing power of ANSYS software, Ansys-LSDyna supports both 2-D and 3-D explicit elements, and features an extensive set of single-surface, surface-to surface and node-to-surface contact as well as a contact analysis option that automatically creates the contact surfaces. Ansys LS-DYNA also gives optional methods for fast solution processing. The symmetric multiprocessing (SMP) and massively parallel processing (MPP) methods optimize the power of multiple CPUs to deliver explicit simulation results in a fraction of the time* [3]."

"*The Abaqus product suite consists of three core products: Abaqus/Standard, Abaqus/Explicit and Abaqus/CAE. Abaqus/Standard is a general-purpose solver using a traditional implicit integration scheme to solve finite element analyses. Abaqus/Explicit uses an explicit integration scheme to solve highly nonlinear transient dynamic and quasi-static analyses. Abaqus/CAE provides an integrated modeling (preprocessing) and visualization (post-processing) environment for the analysis products. The Abaqus products use the open-source scripting language Python for scripting and customization. Abaqus/CAE uses the fox-toolkit for GUI development* [4]."

This paper puts to test, these two software and describes the author's implementation of Ansys LSDyna and Abaqus in solving actual production forging problem.

1.2 Problem Description

The forging process generally consists of heating of the billet material to a specific temperature after which it is deformed plastically by applying forces on the work-piece (billet). At the end of the deformation process the shape of the die is acquired by the work-piece and a desired geometry is obtained. The heating of the work-piece reduces the work hardening effect in the material and makes it more ductile as a result of which less amount of force is required for the operation to be carried out. The forging process is generally accompanied by heat transfer. The work-piece loses heat, and its temperature decreases as the process continues. Heat transfer takes place by conduction, convection and radiation.

The forging problem analyzed in this paper consisted of a circular metal disc bounded on the boundary by a ring die on the top side and a base die on the bottom side. A plunger was enforced to move vertically downwards at the center of the billet. The application of force at the center of the billet while it was restrained at the boundaries, caused it to deform into an inverted dome like shape. The undeformed and deformed shapes of the billet are shown in Figure 1.1 and 1.2 respectively.

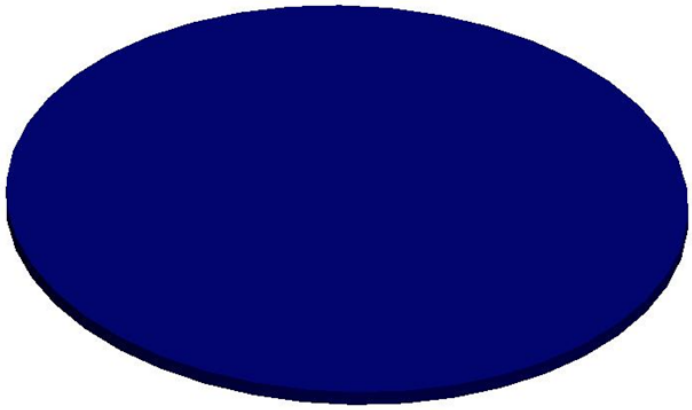

Figure 1.1 Billet Undeformed Shape

Figure 1.2 Billet Deformed Shape

The maximum deformation in the vertically downward direction of the billet found out by experiments[5] was 10.75". The pressure applied by the plunger on the billet gradually increased from 0 to 1950 psi in 19.5 seconds. The billet was 38" in diameter and 0.1875" in thickness. The initial temperature of the billet at the start of the analysis was 1425^0F and reduced to 1200^0F losing heat by conduction, convection and radiation. The initial temperature of the dies was around 300 – 330^0F. The material of the billet was ASME SA 516 Grade 70 while H-26 was used for the dies.

The assembly of the analyzed model along with its cross sectional view is shown below.

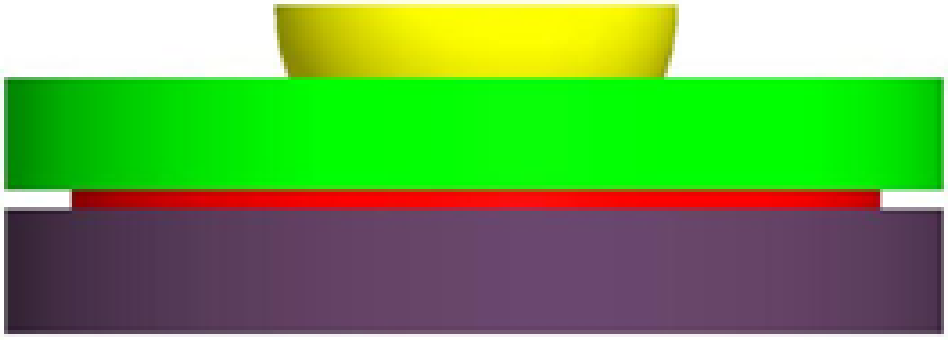

Figure 1.3 Assembly

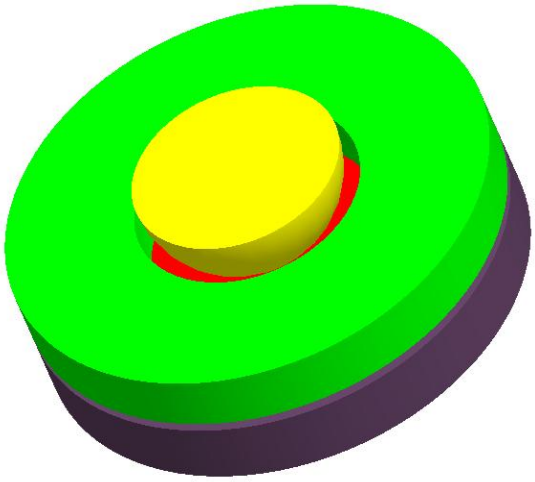

Figure 1.4 Asembly – Isometric View

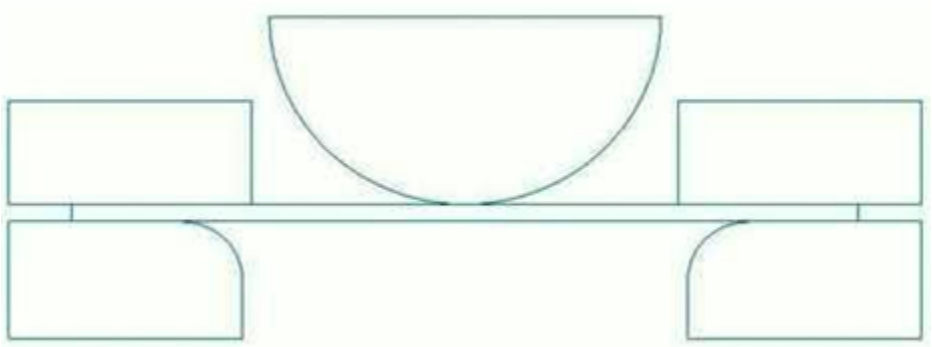

Figure 1.5 Cross Section of the Forging Assembly

1.3 Literature Survey

The finite element methods have been and are being extensively used for the analysis of forging.This section provides information about the implementation of a few finite element codes in handling typical forging problems.

In this paper presented by Ghaei A. and Movahhedy M, Abaqus was used to study the 3D radial forging process and the effects of die shape in the cross-sectional area in deformation. Additionally, the results of 3D model were compared to the results obtained from a 2D axisymmetric model. The results showed that the tube in the radial forging process does not deform axisymmetrically and thus a 3D model is required for such an analysis. The axisymmetric model acts better wihout the mandrel since it is a source of nonhomogeneity [6].

In this paper by Lu H., Wu C. and Xu J. a forging and extrusion analysis was performed with LSDyna. Emphasis was given to the 3D adaptive meshing technique in LSDyna and the state variable transfer between successive discretizations was successfully presented [7].

A paper presented by Zhang Z., Dai G., Wu S., Dong L., and Liu L. simulated the billet upsetting and defect analyses of 42CrMo on DEFORM-3D. The main motive of this study was to study the plastic deformation characteristics of 42CrMo in the upsetting process and to find out the feasibility of DEFORM3D in doing so. The study simulated the stresses, strains, changes in temperatures at different regions of the billet and also proceeded on to analyze the forging defects in the process. The temperature and the stress results obtained complied with the forging practice and theories [8].

In this paper, Wilson W., Schmid S. and Liu J. developed a simple model for heat transfer coefficient between the workpiece and the die in forging operations. Sample hot forging simulations were presented for upsetting ring compression, spike test for Ti-6Al-4V and Rene-88. The analysis was carried out in DEFROM2D. The model required the thermal properties of workpiece, die, the lubricant used and also the fractional contact area and film thickeness. The model showed promising results for different workpiece/tooling and lubrication combinations.The heat transfer is allowed by the model to change according to the process parameters such as film thickness and roughness [9].

Another example of the implementation of the finite element methods in forging is that given by Bang W., Lee C. and Chang Y. In this paper, the flow stress variation due to dynamic recrystallization during hot forging is investigated. Costitutive relations and recrystallization kinematics were formulated from the mechanical test results conducted at various temperatures. A commercial FEM code with conditioned remeshing was used to study the effects of dynamic recrystallization on flow stress. To minimize overestimation of forming loads, the datum strain of stress compensation was optimized. Results showed that implementation of stress compensation to dynamic recrystallization significantly improved forming load prediction by finite element analysis [10].

The remaining chapters in this paper explain the theory of forging accompanied by its software implementation. Chapter 2 deals with the theory of plasticity and its applications. Chapter 3 explains the forgings parameters and the test problems analyzed in Ansys LSDyna and Abaqus. Chapter 4 shows the simulation of the forging of the man-way cover and Chapter 5 discusses conclusions and offers recommendations for future study in this area.

CHAPTER 2

THE THEORY OF PLASTICITY

2.1 The Theory of Plasticity

The metal forming process occurs largely in the plastic range. Plasticity is the study of ductile materials which are permanently deformed by a set of applied forces. It deals with the stresses and strains induced in the material due to permanent deformation. In plasticity, the deformation is determined by the complete history of loading unlike elasticity, where, the deformation depends on the current state of strain under consideration. Thus, the final deformation in plasticity is obtained by the sum of the incremental deformations along the strain path.

A deforming metal becomes more and more anisotropic as the amount of strain hardening increases. Initially, a metal may be considered as isotropic since the crystal grains are distributed in a random manner. But, as the deformation starts, these crystallographic directions gradually rotate towards a common axis making the material anisotropic. Anisotropy is too complex to be successfully incorporated into a theoretical framework and therefore, in the theory of plasticity it is generally assumed that the material remains isotropic throughout the deformation process.

Strain hardening characteristics in an uniaxial stress-strain behavior can be related to that in a complex state of stress. In a single crystal, the plastic deformation is generally produced by slip due to sliding of adjacent blocks of the crystals along planes called as slip planes. The boundary line separating the slipped region of a crystal from the neighboring unslipped region is called a dislocation. Dislocation is caused by a line defect in the crystal causing a local concentration of stress. Slip usually occurs on planes having a comparatively high concentration of atoms. The grain boundaries between crystallites in a polycrystalline

metal act as effective barriers to slip. As the deformation continues, the dislocations pile up along the slip planes at the grain boundaries opposing the generation of new dislocations. These dislocations start moving across the boundary once the applied stress increases to a critical value.

The strain hardening in a metal is caused due to the dislocation pile-up in the early stages of the plastic deformation. In polycrystalline metals, as the yield strength increases due to the dislocations interacting with one another and also with the foreign atoms serving as barriers, the rate of strain hardening is always greater as compared to that in a single crystal. The dislocation interactions control the yield strength of a polycrystalline metal only in the later stages of the deformation.

The process in which the ductility of the material is restored by increasing its temperature is called as annealing. If the temperature of the strain-hardened metal is progressively increased, the strain-hardened state becomes unstable, and the material eventually reverts to the unstrained state thus decreasing the dislocation density considerably. The temperature at which the cold work state is replaced by a new set of strain free grains is known as the re-crystallization temperature [11].

2.2 Applications of the Theory of Plasticity

Metal working processes constitute of large plastic strains and form an important area of application of the theory of plasticity. The significance of mechanical tests such as the hardness test and the notch tensile stress test cannot be fully appreciated without a knowledge of the extent of the plastic zone and the associated state of stress. Many problems have to deal with elastic and plastic strains comparable in magnitude arising when the loading is continued beyond the elastic limit. The theory of plasticity can be put to good use in such structural problems. As the plasticity theory takes full advantage of the available ductility of the material, structural designs based on the estimation of collapse loads are more economical than elastic designs [11].

2.3 Stress-Strain Behavior

When the true stress (σ) is plotted against true or natural strain (ε), the stress-strain curve of an annealed material in simple tension and in simple compression is found to coincide with each other. Figure 2.1 shows the true stress–strain curve of a typical annealed material in simple tension. As long as the applied stress is below the yield strength, the material behaves elastically and when the applied load is removed, the specimen regains its original size. In the figure, the slope of the line *OA* is known as Young's modulus. At point *A*, the linear relationship between the stress and the strain ceases to exist and is known as the proportionality limit of the stress-strain relationship. The elastic range generally extends slightly beyond the proportionality limit.

The point *B* on the stress-strain curve is known as the yield point. The location of the yield point *B* is largely a matter of convention, since the transition from elastic to plastic behavior in most metals is gradual. The stress corresponding to the yield point *B* is called as the yield stress *Y*, and is defined as the amount of stress for which a small amount of permanent deformation is observed in the metal.

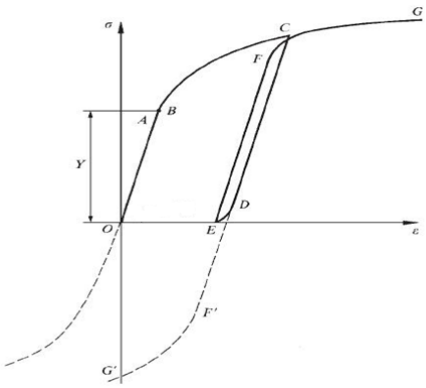

Figure 2.1 The Stress-Strain Curve with Effects of Unloading [11]

As seen from the Figure 2.1, the stress continually increases with plastic strain beyond the yield point, while the slope (representing the rate of strain hardening) decreases with increasing stress. At any point *C* on the stress-strain curve in the plastic range, if the load is completely removed, there is an elastic recovery along the path *CD* intersecting the strain axis

at point *E.* The plastic strain at this stage is represented by the line *OE*. Reapplication of the load, leads to the specimen deforming elasticity until a new yield point *F* is reached. Generally, the hysteresis loop formed during the unloading and loading of the load is neglected and *F* is considered to be coincident with *C.* The stress-strain curve proceeds along *FG* on further loading as a continuation of curve *BC*. The curve *EFG* can be regarded as the stress–strain curve of the metal prestrained by the amount *OE*. A greater degree of prestrain leads to a higher yield point and a flatter strain-hardening curve. Material is said to be nonhardening or ideally plastic when the rate of strain hardening is very small due to a highly prestrained state [11].

CHAPTER 3

FORGING PARAMETERS

3.1 Forging Parameters

Plastic deformation and friction, both, lead to heat generation in metal forming processes. The mechanical energy involved in the forging process transformed into heat accounts for almost 90 – 95%. Temperature increases of several hundred degrees are seen in forming operations such as drawing and extrusion which are performed at high speeds. In high-speed forging equipments such as mechanical press, screw press, and hammer, heat generation is considered as a significant phenomenon. Some part of the heat generated during a forming process dissipates into the undeformed portion of the deforming metal and the tools which are in contact with that metal, while some part of the heat remains in the deformed portion. Lubrication conditions, tool life, microstructure and the properties of the forged part are affected due to the temperatures developed in the forging operation.

With the advent of finite element analysis, the heat generation phenomenon, influence of press speed, contact time, and heat transfer in metal forming can be reasonably simulated in a computer. Parameters like the work-piece and the die interface heat transfer coefficient, thermal convection coefficient, emissivity must be known to ensure accurate heat transfer calculation.

In metal forming, the heat transfer process mainly depends on:

a. The initial work-piece temperature
b. The initial die temperatures
c. Inelastic heat generation
d. Heat generation due to friction at the work-piece/die interface
e. Contact conductance

f. Coefficient of thermal convection

In a metal forming process, the average instantaneous temperature in the deforming work-piece, T, can be calculated by,

$$T = T_w + T_d + T_f - T_t - T_r - T_c \quad (3.1)$$

where,

T_w = the initial temperature of the work-piece,

T_d = the temperature rise due to inelastic deformation,

T_f = the temperature rise due to friction,

T_t = the temperature drop due to contact conductance,

T_r = the temperature drop due to thermal radiation,

T_c = the temperature drop due to convection [12].

3.2 Influence of Press Speed and Contact Time on Heat Transfer

The forging equipment used in the process of forging can also be said to have a significant influence in a metal forming operation affecting the heat transfer and hence the temperature history of the work-piece. The hydraulic presses used in the metal forming analysis have lower speeds and thus lower strain rates while the mechanical and screw presses have higher speed leading to higher strain rates during deformation. In hydraulic presses, the slower speeds lead to a longer dwell time before deformation whereas, the mechanical and screw presses owing to their high speed have a lesser dwell time resulting in a longer free resting heat transfer between the work-piece and the dies in case of hydraulic presses and a less amount of heat transfer in mechanical and screw presses.

In metal forming, intermittent contact conditions exist between the work-piece and the die. The temperatures in a forming process are influenced greatly by the length of the contact time. The contact time under pressure is the most important factor influencing temperatures in hot forging processes [12].

3.3 Test Problems

The test problems given below demonstrate the use of the aforementioned softwares in plasticity problems.

3.3.1 Test Problem 1

3.3.1.1 Overview

This test problem deals with the classic plasticity example of a rectangular cross-sectioned beam subjected to a bending moment as shown in Figure 3.1. The theory successfully derives a relationship between M, the bending moment causing inelastic deformation in the fibers of the beam and M_e, the bending moment causing elastic deformation. This paper makes an attempt to exploit this relation using Ansys LSDyna and Abaqus software packages [13].

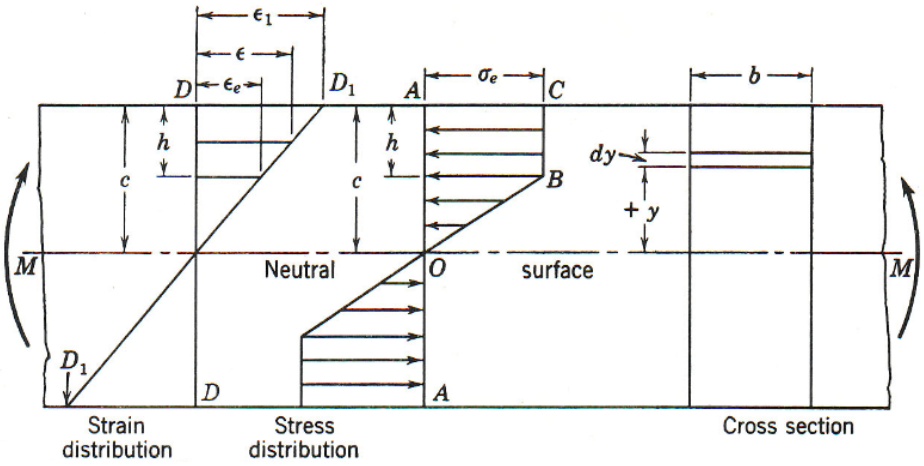

Figure 3.1 Bending of a Rectangular Cross Sectioned Beam [13]

A straight beam having a rectangular cross-section was assumed to be made of a material having a stress-strain curve as shown in Figure 3.2.

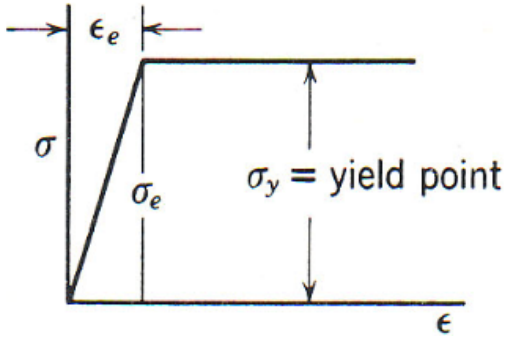

Figure 3.2 Stress-Strain Curve [13]

The material had a yield point σ_e. The compression stress-strain curve was identical with the curve found in the tension test. M was assumed to be the bending moment corresponding to any given depth h of inelastic yielding in the fibers of the beam, and M_e, the bending moment causing inelastic deformation in the outermost fiber to start ($M_e = \sigma_e I/c$).

3.3.1.2 Dimensionless Moment-Depth of Plastic Strain Equation

The dimensionless Moment-Depth of Plastic Strain Equation of the beam is given by,

$$M/M_e = 1 + (h/c) - \tfrac{1}{2}(h^2/c^2) \qquad (3.2)$$

A portion of the beam having ordinates as the ratios of M/M_e and h/c and $\varepsilon_1/\varepsilon_e$ as the upper and lower abscissa values respectively is shown rotated 90° for convenience in Figure 3.3

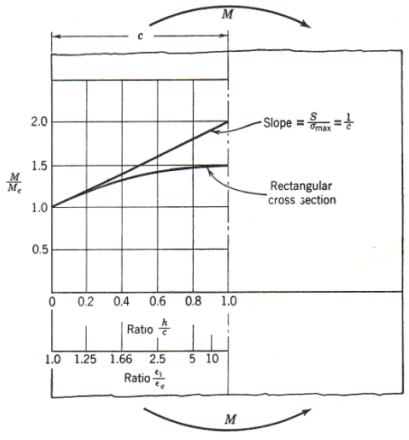

Figure 3.3 M/M_e vs. h/c, $\varepsilon_1/\varepsilon_e$ [13]

The outer fibers of the beam are on the verge of straining inelastically at an abscissa value of h/c = 0 and the fibers of the beam can be said to have been strained inelastically throughout the entire depth of the beam at h/c = 1. From the moment – depth equation, when h/c =1, $M/M_e = 1.5$. So, at h/c = 1, the ratio of M/M_e is referred to as fully plastic.

3.3.1.3 Dimensionless Moment-Strain Equation

The dimensionless Moment-Strain Equation of the beam is given by,

$$M/M_e = 3/2 – 0.5/ (\varepsilon_1/\varepsilon_2)^2 \quad (3.3)$$

As stated earlier, the ratio $\varepsilon_1/\varepsilon_e$ is represented on the lower scale of abscissa in Figure 3.3. It can be seen, that when the ratio $\varepsilon_1/\varepsilon_e = 1.25$, the value of $M/M_e = 1.2$ approximately [13].

3.3.1.4 Software Simulation

The beam under consideration had a rectangular cross section 0.5 in. wide and 0.375 in. deep. It was made up of mild steel following the stress-strain curve shown in Figure 3.2. The yield strength and the Young's Modulus of the material were 30,000 and 30,000,000 psi respectively. The elastic strain was given by $E_e = \sigma_e/E = 0.001$ and the elastic bending moment $M_e = \sigma\ I/c = 352$ ld-in.

The aim of the simulations was to get the M/M_e ratio in accordance with the dimensionless moment strain equation.

3.3.1.4.1 Ansys LSDyna

Due to the quasi-static nature of the problem, there was no need for a dynamic analysis and hence the problem was solved completely in Ansys itself. A symmetric model meshed with Plane42 elements was used. The beam model consisted of 2208 elements. One end of the beam was constrained using the symmetry boundary conditions and a uniformly varying load was applied at the other end to represent the bending moment.

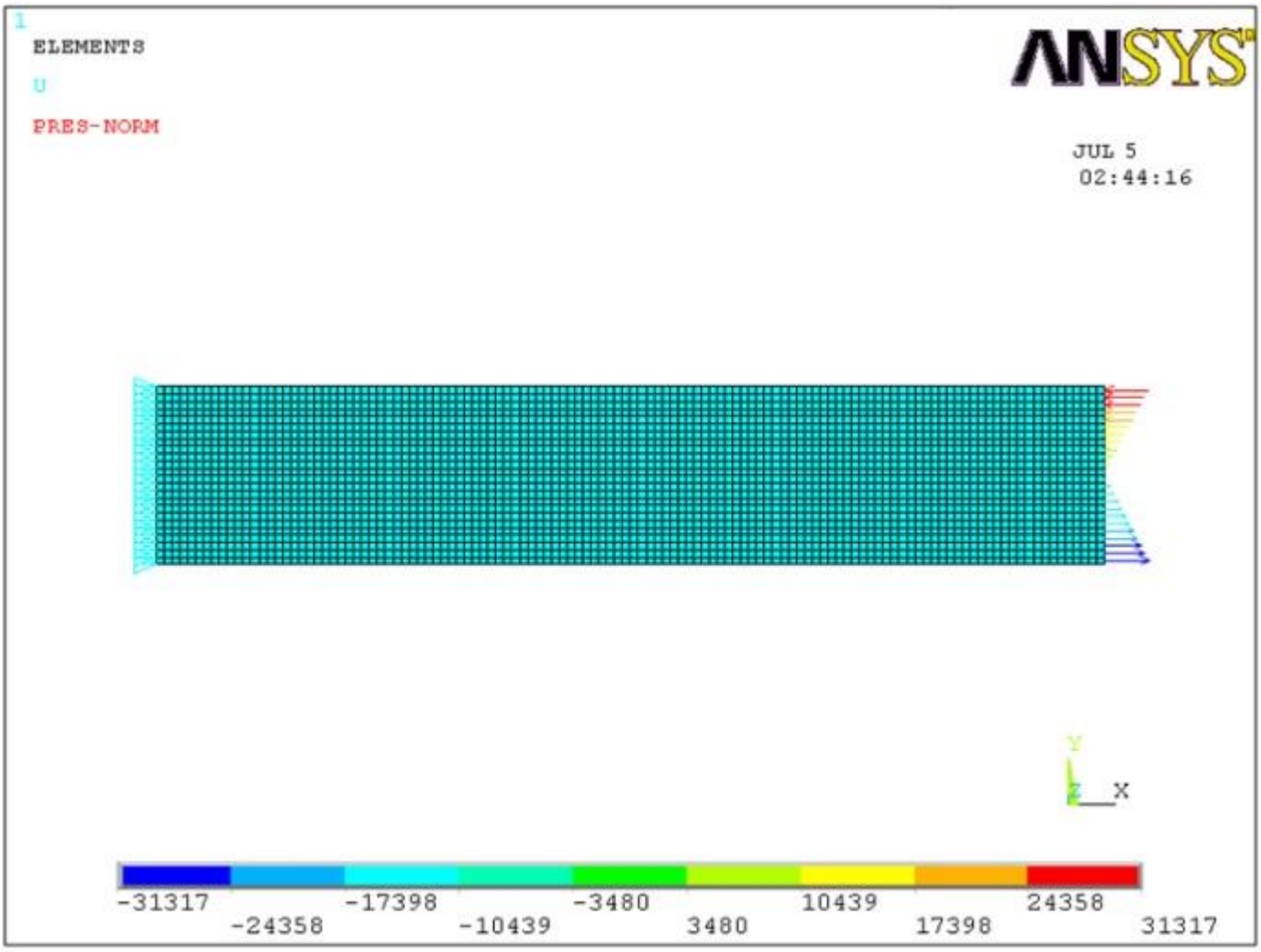

Figure 3.4 Beam Model (Ansys)

A bending moment in the form of uniformly varying triangular load was applied to the beam in such a way that it did not exceed the load required to cause any structural damage. The uniformly varying load was applied using the function editor in the Ansys pre-processor as shown in Figure 3.5.

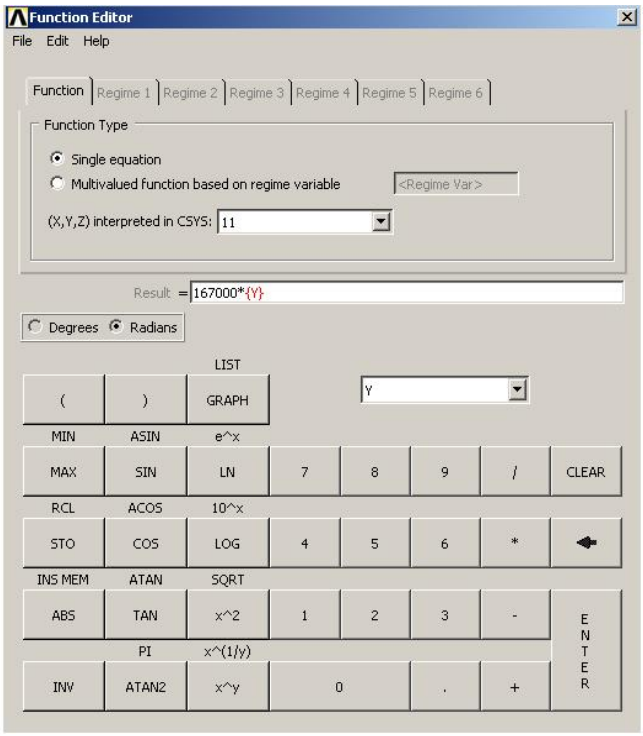

Figure 3.5 Ansys Function Editor

The stress results obtained were in accordance with Figure 3.1.

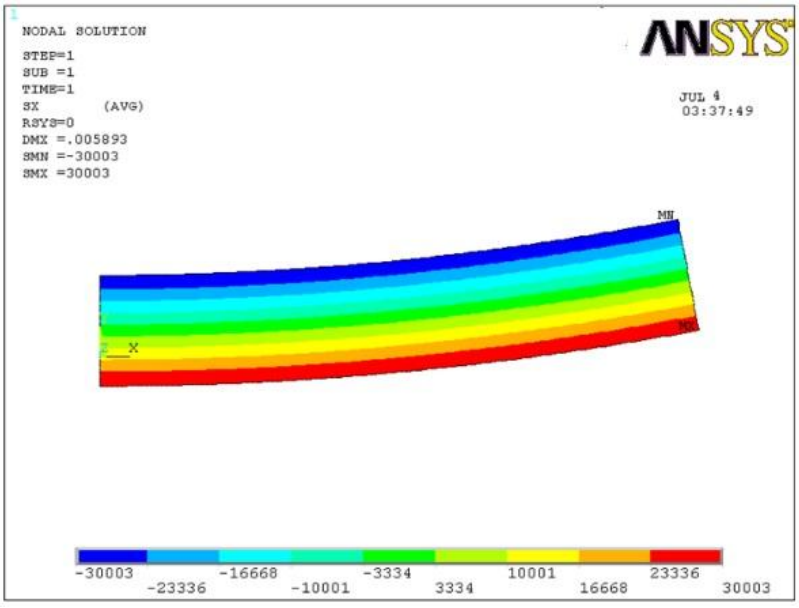

Figure 3.6 Stress Results (Ansys)

As seen, the maximum stress in the outermost fibers (in tension) was approximately equal to the yield strength of the material. The h/c ratio used was 0.044. For this ratio, the bending moment (M) was calculated as 367lb-in and M/M_e was calculated as 1.0426 from equation 3.2. The total strain plot is shown in Figure 3.7.

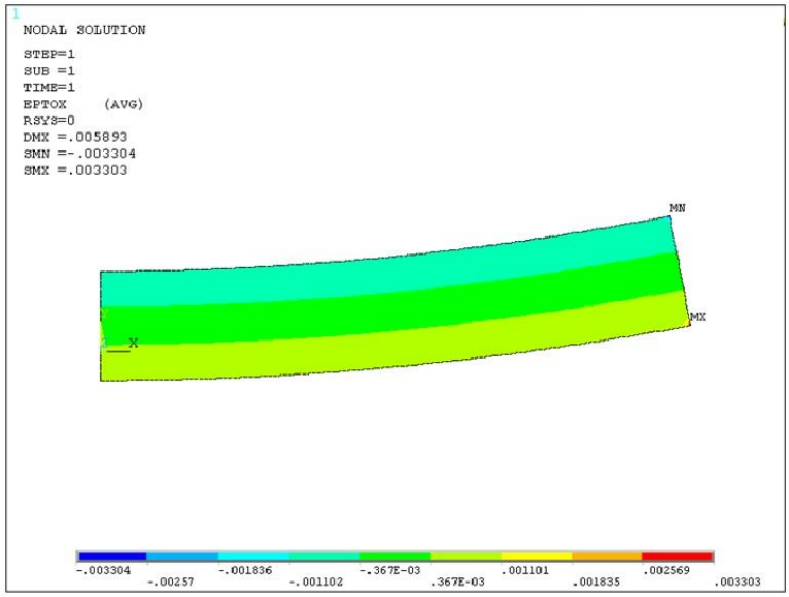

Figure 3.7 Total Strain Results (Ansys)

As can be seen from Figure 3.7, the inelastic strain at the outermost fibers in the deformed model was approximately equal to 0.0011.

The inelastic to the elastic strain ratio ($\varepsilon_1/\varepsilon_e$) was thus found out to be 1.1. From equation 3.3, for $\varepsilon_1/\varepsilon_e$ equal to 1.1, M/M_e was back calculated, and was found out to be equal to 1.04, thus justifying the Ansys simulation results.

3.3.1.4.2 Abaqus

The symmetric model in Abaqus was similarly constrained at one end and a varying pressure was applied at the other using the load module. The beam was modeled with CPS4R (A 4 node bilinear plane stress quadrilateral, reduced integration) and it consisted of 2101 elements.

A constrained model is shown in Figure 3.8 below.

Figure 3.8 Beam Model (Abaqus)

The stress results of the Abaqus simulation are shown in Figure 3.9.

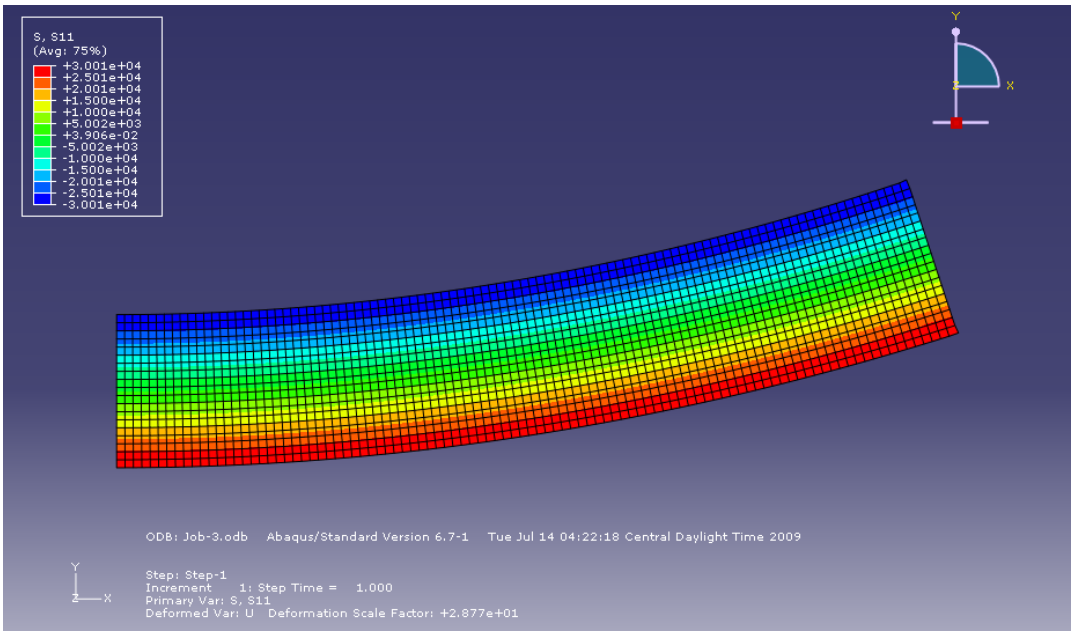

Figure 3.9 Stress Results (Abaqus)

Here again, the maximum stresses in the fibers in the plastic region were found to be equal to the yield strength as expected. An h/c ratio of 0.068 was used for which the ratio of M/M_e calculated from equation 3.2 was 1.08. The total strain plot for the Abaqus simulation is shown below.

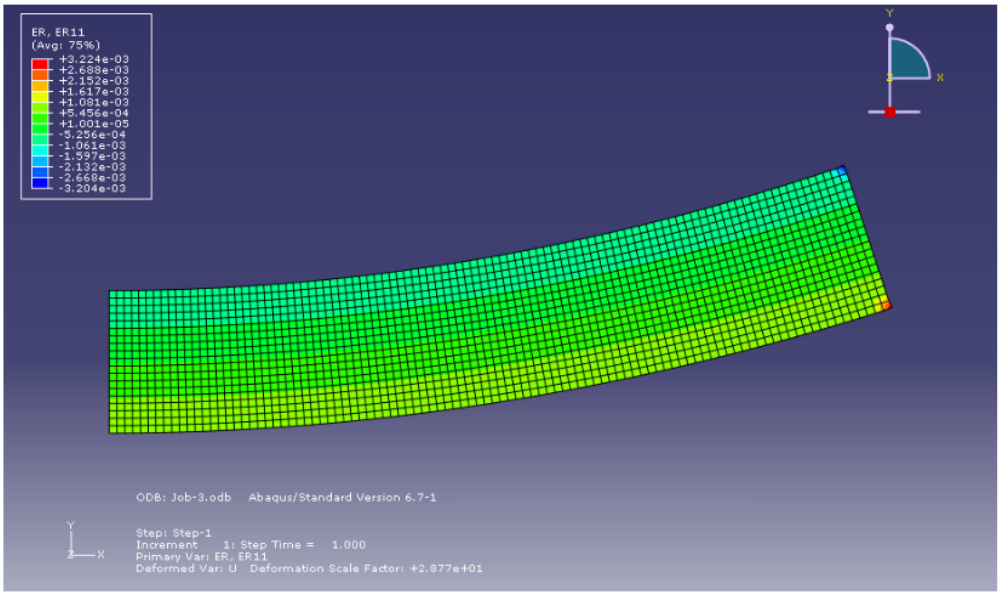

Figure 3.10 Total Strain Results (Abaqus)

The inelastic strain found in the outer fibers of the beam was $1.081e^{-3}$.The ratio $\varepsilon_1/\varepsilon_e$ thus calculated was 1.087. From equation 3.3, M/M_e was found out to be 1.077. The beam bending simulation in Abaqus showed good agreement with the theory.

3.3.2 Test Problem 2

This study was performed by Mary Wicklin Schleider at the Mercer University Engineering Research Center in 1994 using MSC/DYNA. In this study the phenomenon of die filling in the forging process was investigated [14].

3.3.2.1 Three Dimensional Simulation of a Closed Die Forging Process

An H-shaped die and a rectangular parallelepiped billet were modeled to demonstrate flashless forging with fully filled die. The material flow around sharp corners was studied using the H-shaped cross-sectioned die.

Figure 3.11 3D Forging Assembly – Front View

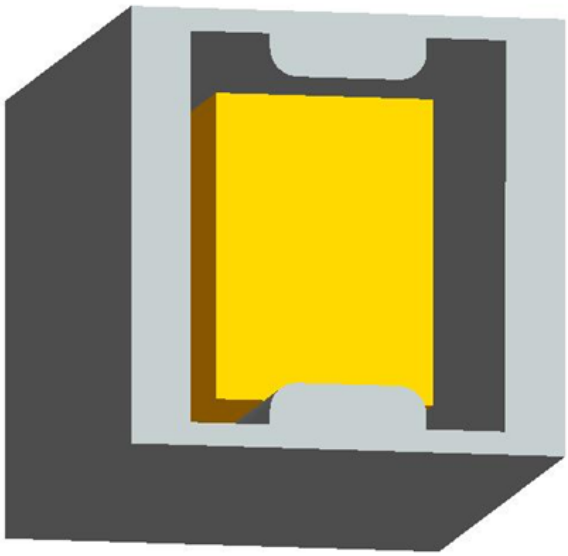

Figure 3.12 3D Forging Assembly – Isometric View

To achieve flashless forging, the volume of the cavity of the die was kept equal to that of the billet, so at full closure of the die on the billet, the die cavity would be completely filled. A constant velocity of 760 in/sec as used the MSC/DYNA simulation was imposed on the top die so that it moved downwards applying pressure on the billet and deforming it as the process continued.

This model incorporated isotropic hardening, and the Young's modulus, yield stress, and the hardening modulus were specified.

The billet was positioned relative to the die cavity in such a way that the material within the die cavity would move in all the three directions thus producing a three-dimensional flow pattern. The billet material flow was studied as it filled the die.

The value of the friction coefficient between the contact surfaces of the die and the billet was maintained as a constant, present whenever a surface of the die touched a surface of the billet.

The material properties modeled were:

$E = 10 \times 10^6$ psi (modulus of elasticity)

$E_h = 10 \times 10^3$ (hardening modulus)

$\upsilon = 0.33$ (Poisson's ratio)

$\eta = 0.5$ (coefficient of friction)

$\rho = 2.64 \times 10^{-4}$ lb-sec^2/in.in^3 (mass density)

$\sigma = 90{,}000$ psi (yield stress)

A comparison of the die force required to move a specific distance was made. Total forces were plotted for various die displacements.

Table 3.1 Die Displacement & Force

Die Displacement (IN)	Force (LB) (Thousands)
0.3	-120
0.5	-115
0.7	-120
0.9	-130
1.1	-380

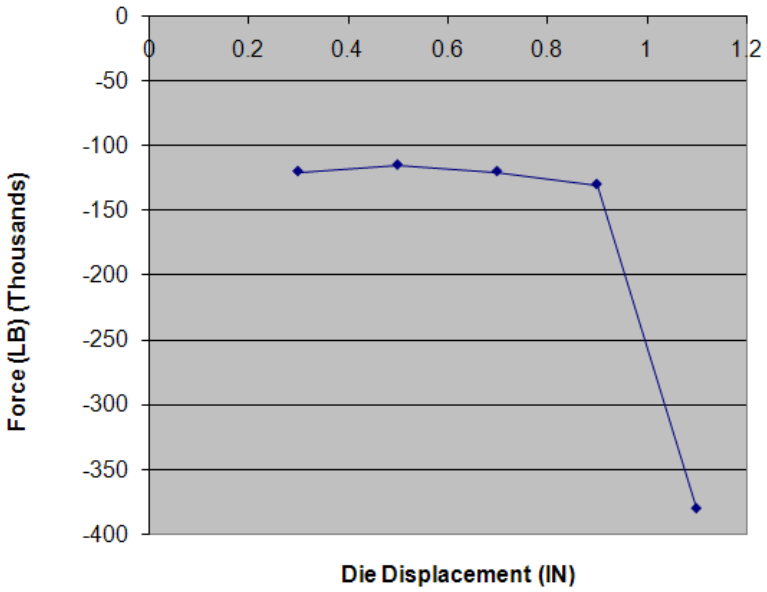

Figure 3.13 Force vs. Displacement

This three-dimensional simulation was performed in this thesis with the intention of matching the results shown in Figure 3.12. A dimensioned sketch of the H-shaped die and the billet is shown below.

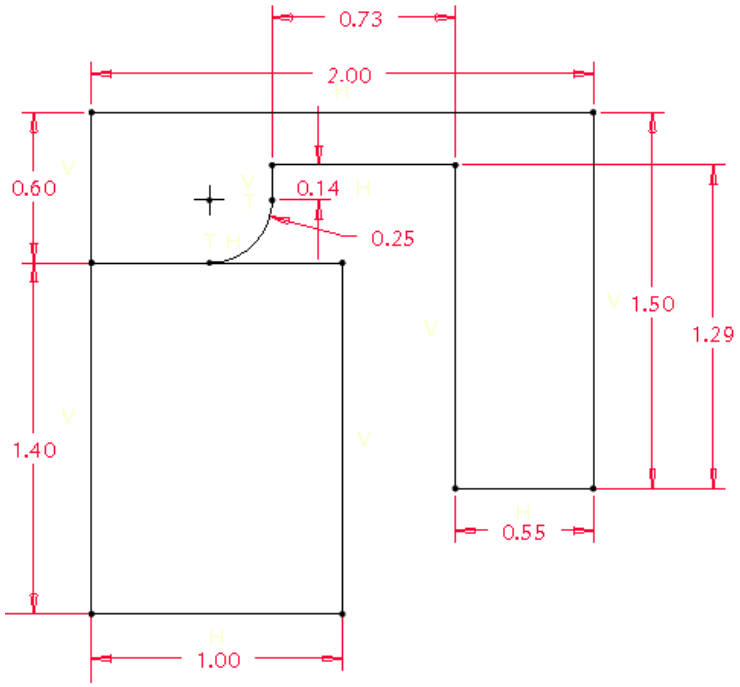

Figure 3.14 One/Eighth Portion of the 3D Forging Assembly

The billet and the die had depths of 1.607” and 2.9” respectively.

3.3.2.2 Software Simulation

3.3.2.2.1 Ansys LSDyna

For the three dimensional simulation, the model was meshed with Solid162 elements. The number of elements used was 17843. Only one-eighth of the die and the billet were modeled due to symmetry. The rear, left and the bottom surfaces of the billet represented the planes of symmetry and the nodes on these surfaces were constrained from moving across these planes. A bilinear isotropic material was defined for the billet whereas the die was defined as rigid, constrained to move in the X and Z directions as shown.

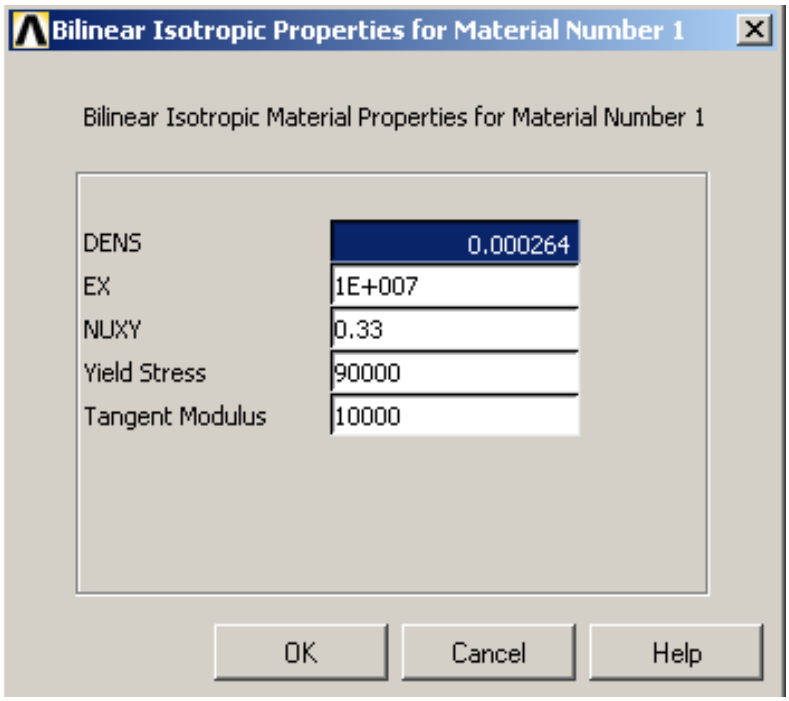

Figure 3.15 Bilinear Isotropic Material Properties

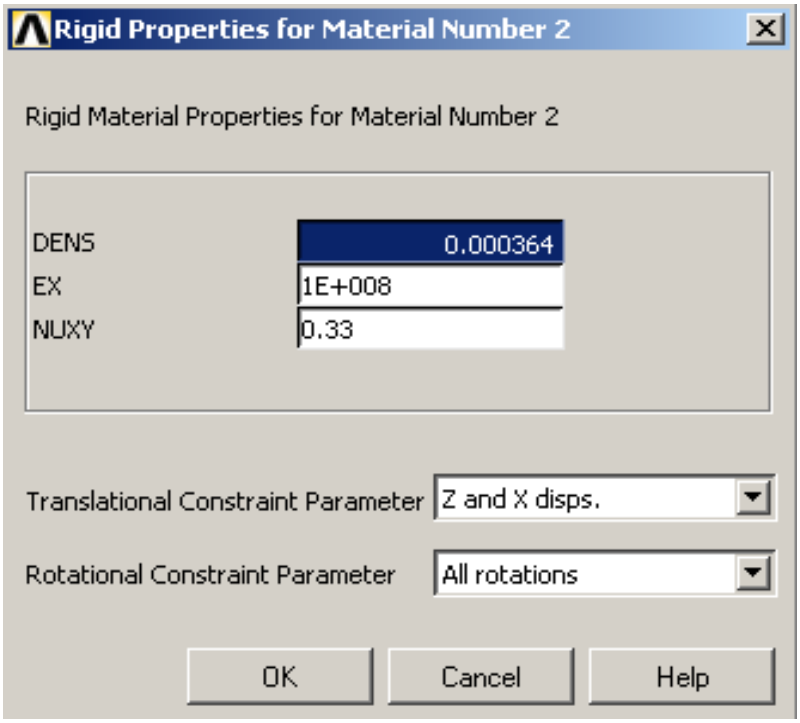

Figure 3.16 Rigid Material Properties

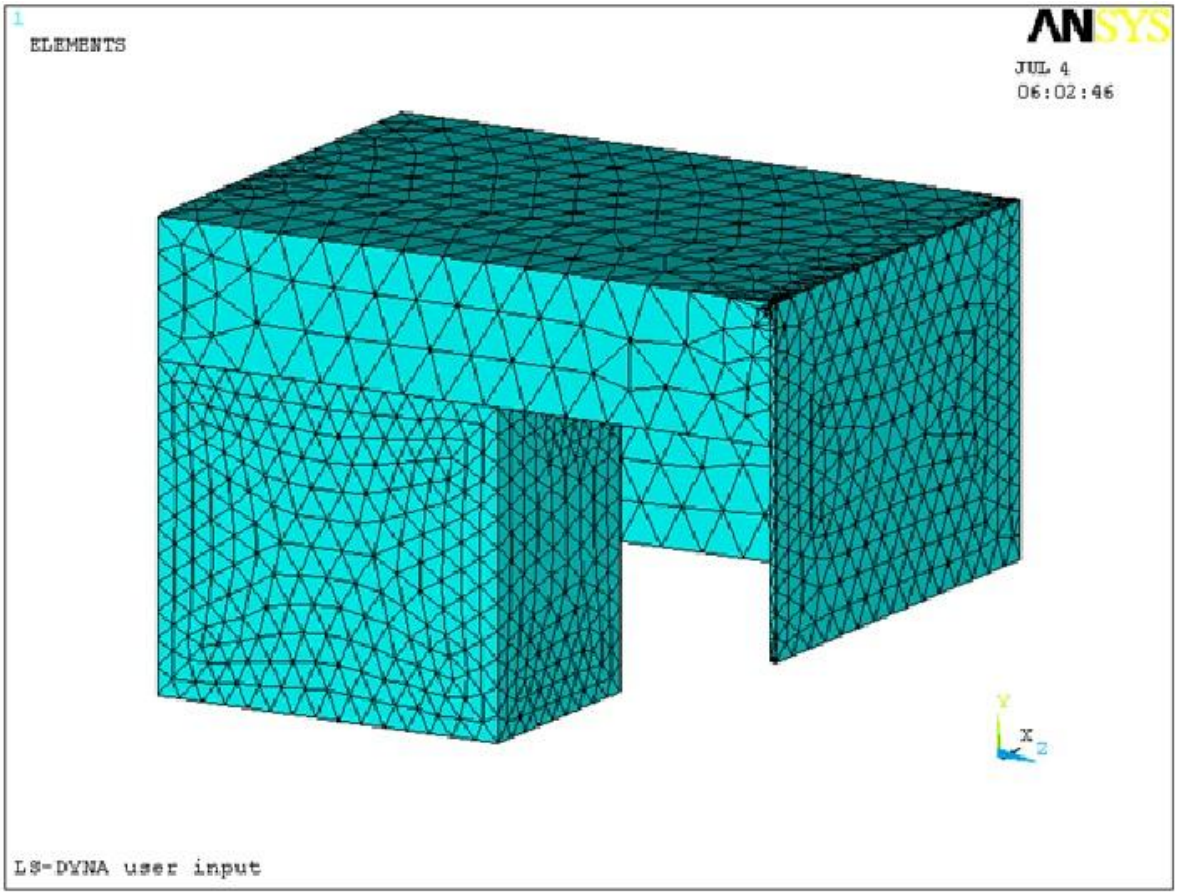

Figure 3.17 Forging Model (Ansys LSDyna)

A single surface, automatic general contact was defined between all the contacting surfaces. In such type of contact, Ansys LSDyna automatically determines which surfaces within a model may come into contact. This option is very powerful for large deformation problems. The static and the dynamic coefficients of friction were maintained at 0.5. The figure below shows the contact parameter definition box in Ansys LSDyna.

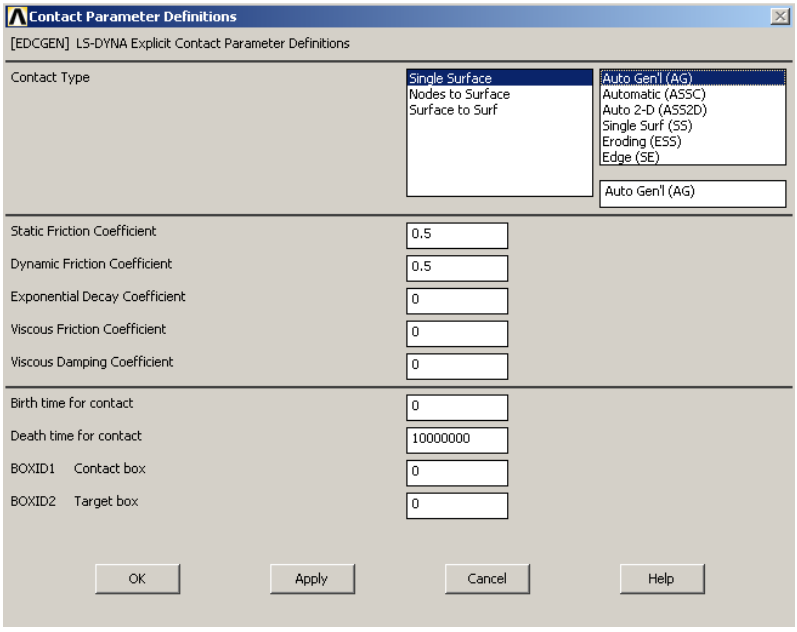

Figure 3.18 Contact Parameter Definition

The velocity of 760 in/sec was applied to the die in the negative Y direction by the EDLOAD command.

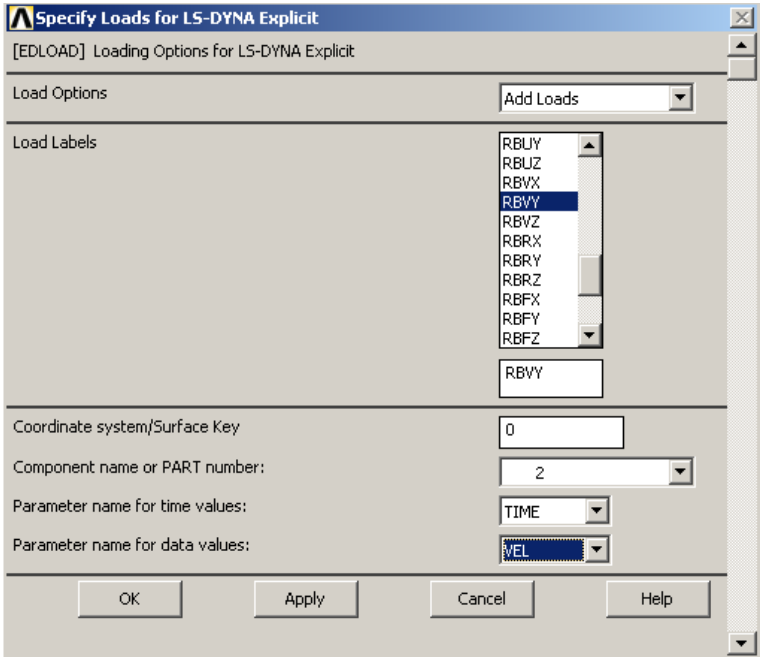

Figure 3.19 The EDLOAD Command Box

The simulation was carried out for a die displacement of 1.1 inches and the stress distribution in the Y (vertical) direction was studied at every regular interval of 0.2 in. starting from 0.3 in. The figures below show the deformation process of the billet at die displacements of 0.3, 0.5, 0.7, 0.9 and 1.1 in.

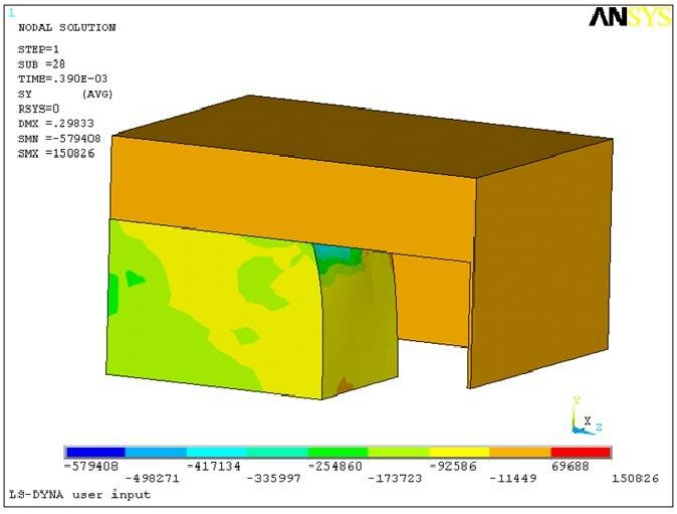

(a)

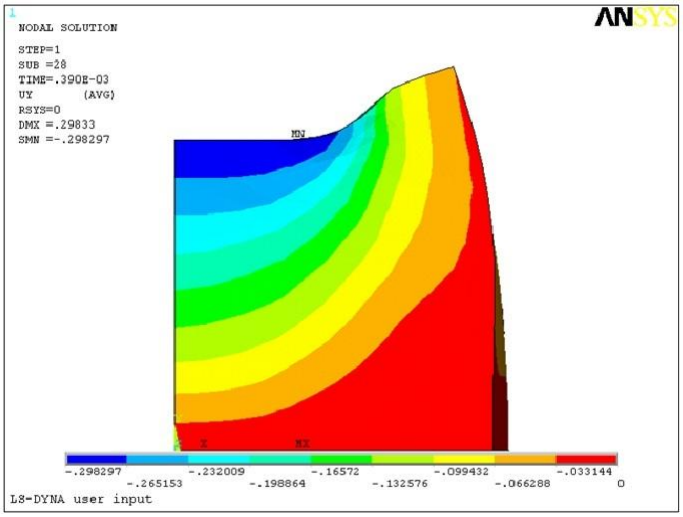

(b)

Figure 3.20 Deformed Shape at 0.3” Die Displacement (Ansys LSDyna) (a) Isometric View, (b) Front View

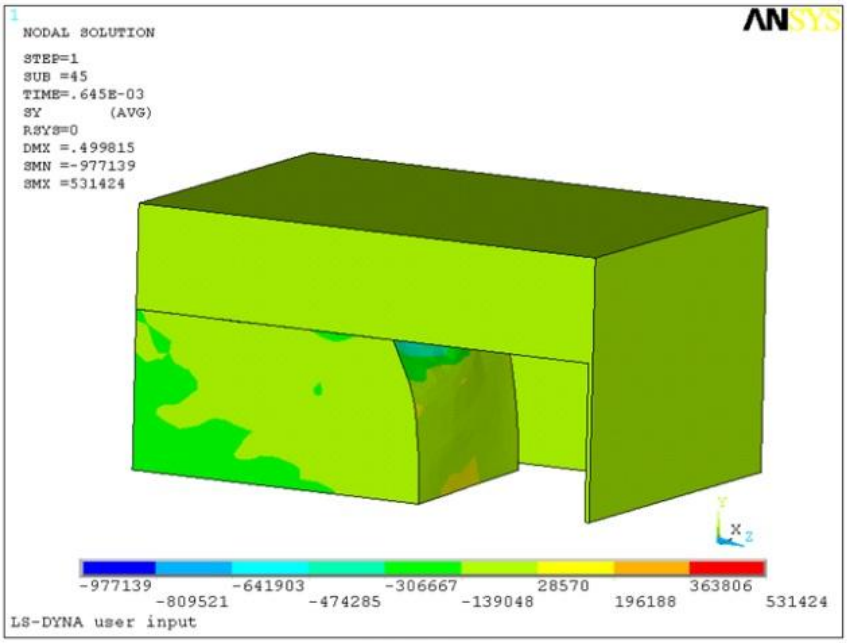

(a)

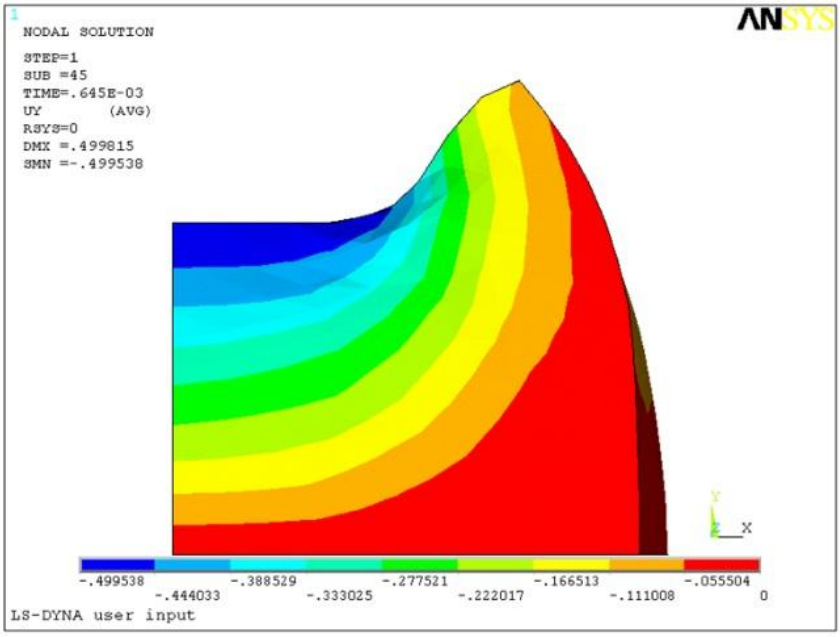

(b)

Figure 3.21 Deformed Shape at 0.3” Die Displacement (Ansys LSDyna) (a) Isometric View, (b) Front View

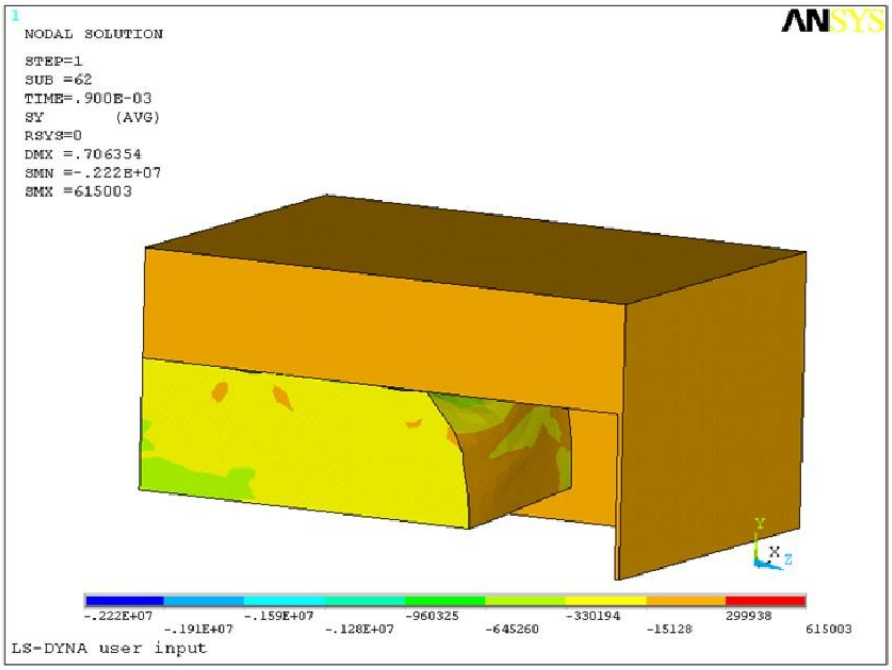

(a)

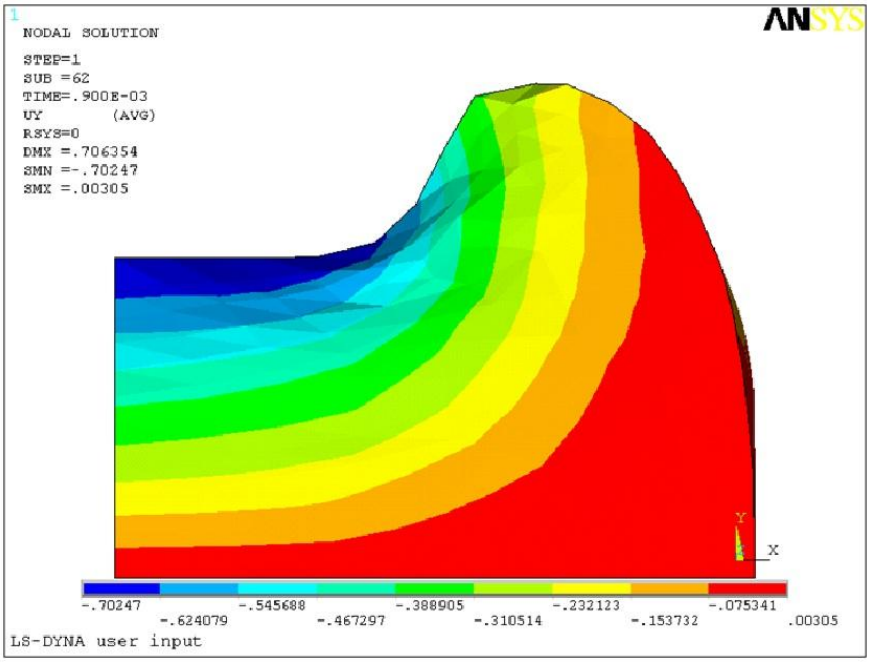

(b)

Figure 3.22 Deformed Shape at 0.3” Die Displacement (Ansys LSDyna) (a) Isometric View, (b) Front View

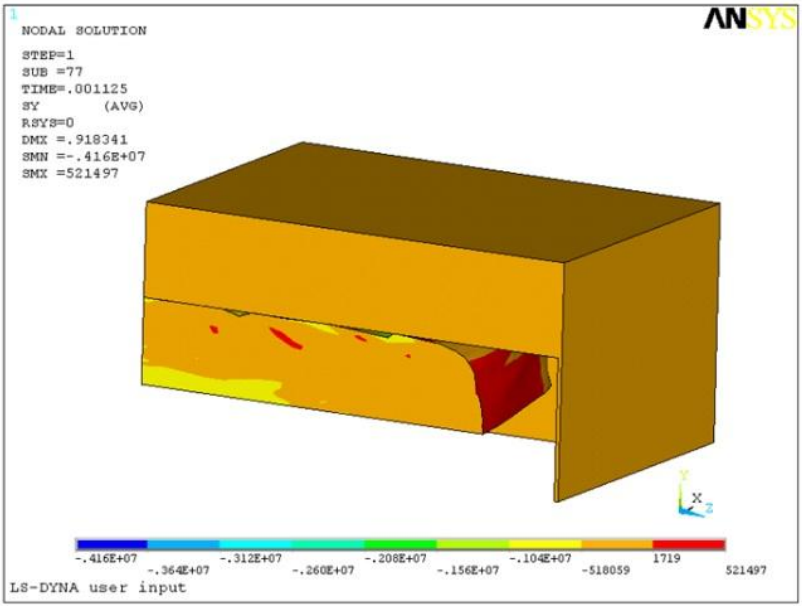

(a)

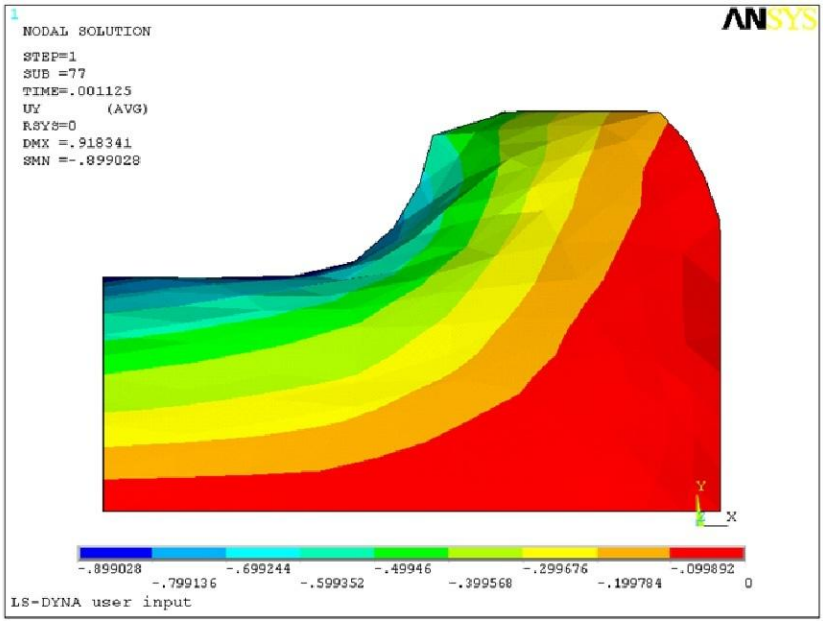

(b)

Figure 3.23 Deformed Shape at 0.3” Die Displacement (Ansys LSDyna) (a) Isometric View, (b) Front View

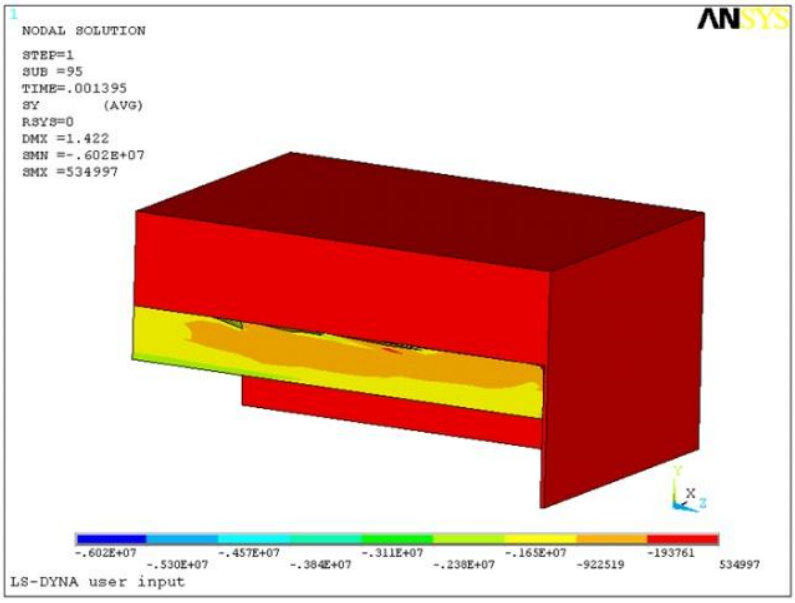

(a)

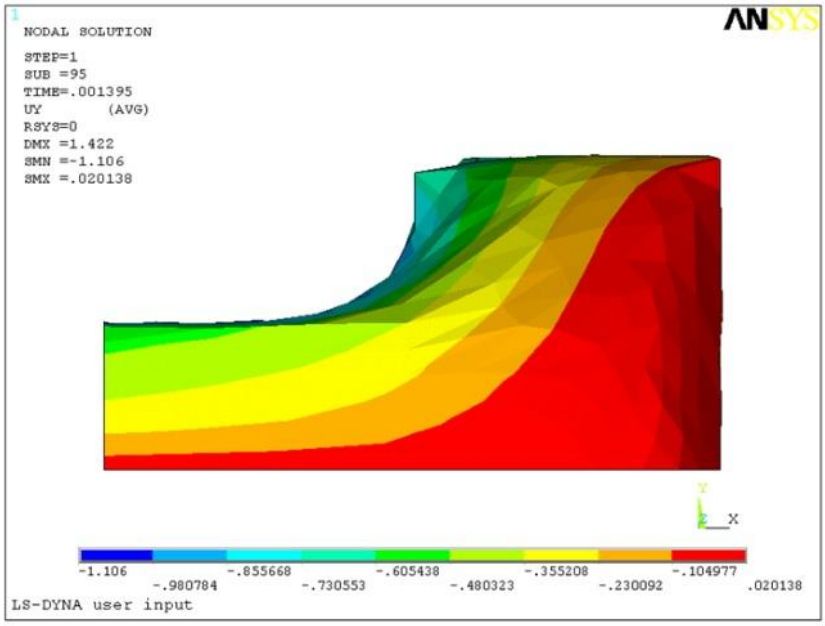

(b)

Figure 3.24 Deformed Shape at 0.3” Die Displacement (Ansys LSDyna) (a) Isometric View, (b) Front View

The Ansys LSDyna force versus displacement results are shown below.

Table 3.2 Die Displacement & Force (Ansys LSDyna)

Die Displacement (IN)	Force (LB) (Thousands)
0.3	-130
0.5	-130
0.7	-140
0.9	-150
1.1	-450

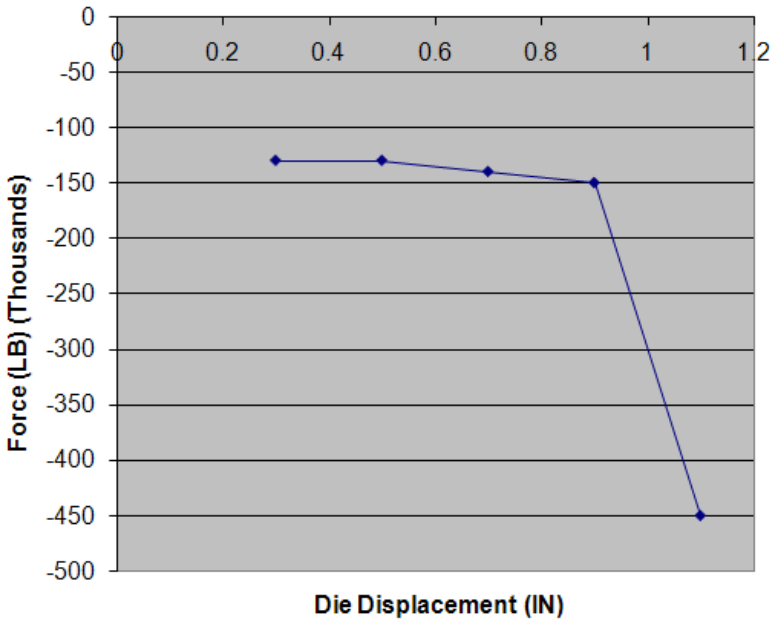

Figure 3.25 Force vs. Displacement (Ansys LSDyna)

The results matched closely with those given in Figure 3.12. The slightly higher forces can be accounted by the difference in the mesh and the element type used.

3.3.2.2.2 Abaqus

A C3D8R (Continuum 3-D 8 Node Reduced Integration) element was chosen for the analysis. The number of elements was 19922. The die was defined as rigid using the rigid body constraint option and was constrained to move in the X and Z directions. The rear, left and the bottom surfaces of the billet represented the planes of symmetry as before and were constrained from moving across their respective planes by using the boundary condition option. The velocity 760 in/sec was specified to the die using the velocity boundary condition. The simulation was carried out until the die displacement of 1.1 in. in the negative Y direction. The process was defined as dynamic, explicit.

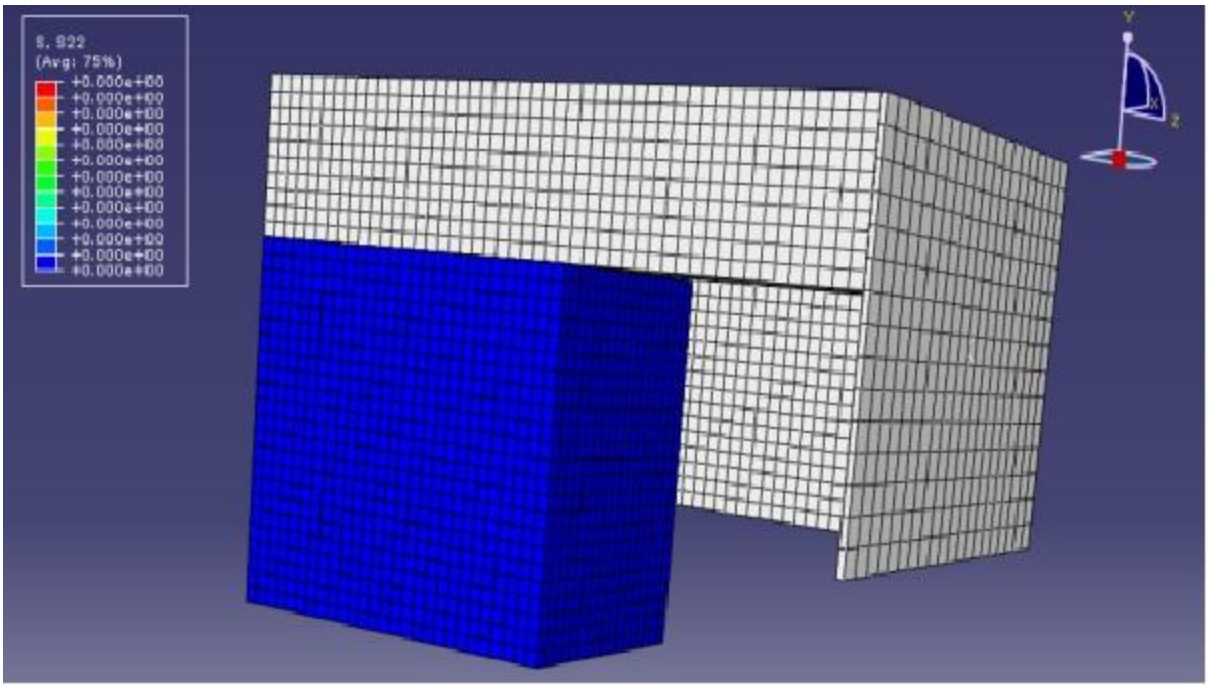

Figure 3.26 Forging Model (Abaqus)

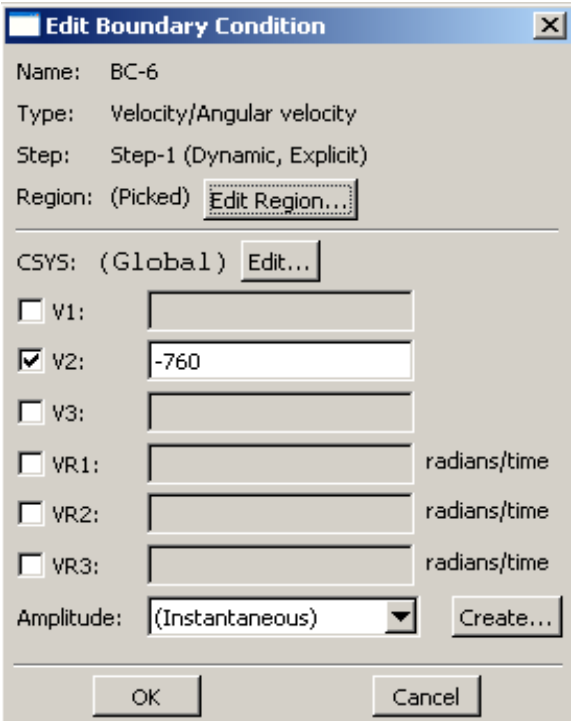

Figure 3.27 Velocity Boundary Condition

The stress distribution in the Y direction is shown below for displacements of 0.3, 0.5, 0.7, 0.9, and 1.1 in.

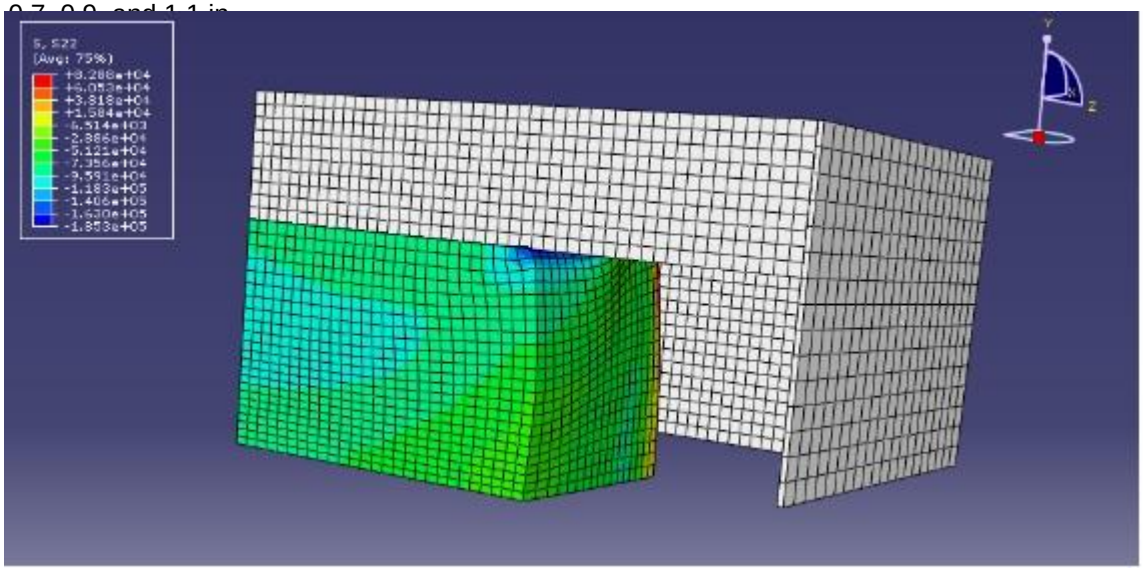

Figure 3.28 Deformed Shape at 0.3" Die Displacement (Abaqus)

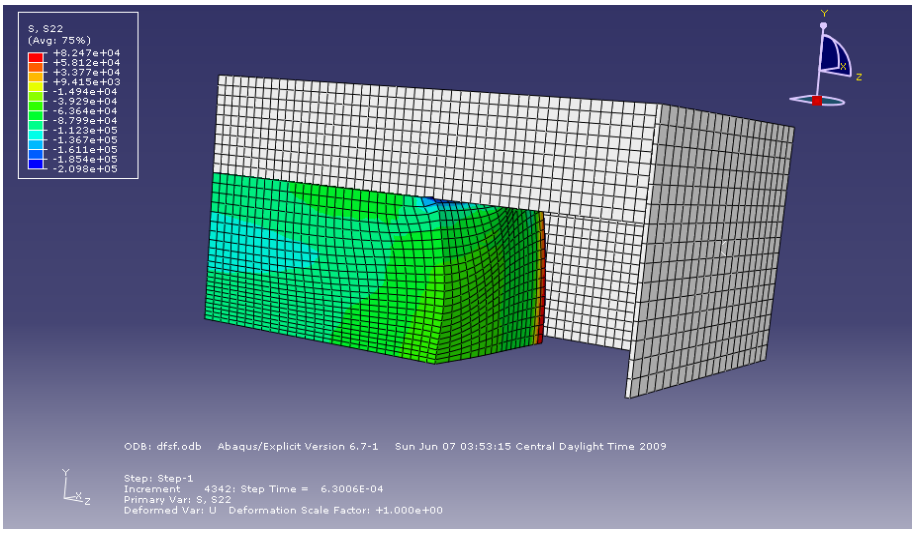

Figure 3.29 Deformed Shape at 0.5” Die Displacement (Abaqus)

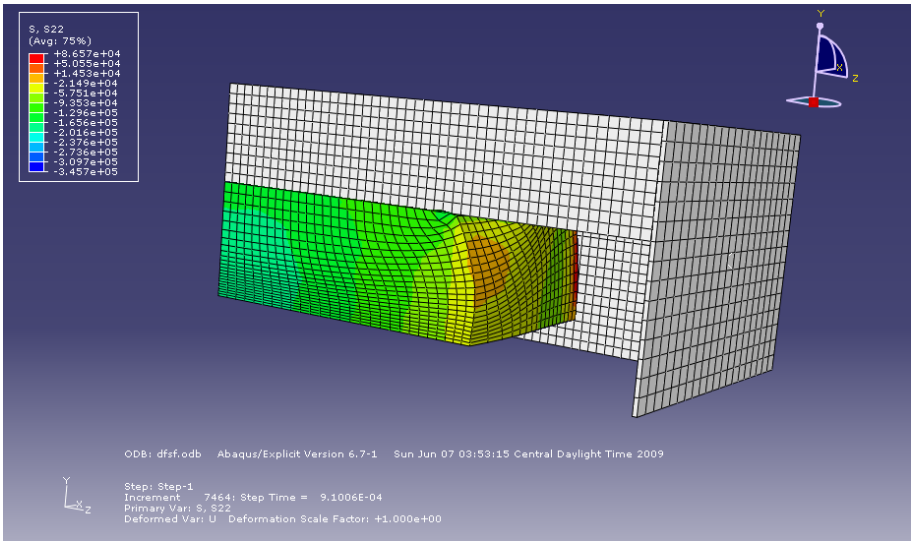

Figure 3.30 Deformed Shape at 0.7” Die Displacement (Abaqus)

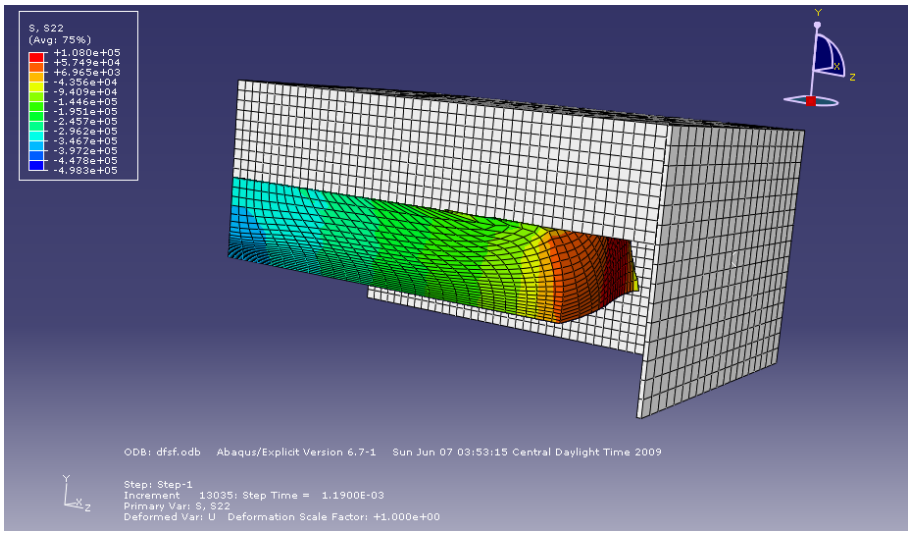

Figure 3.31 Deformed Shape at 0.9” Die Displacement (Abaqus)

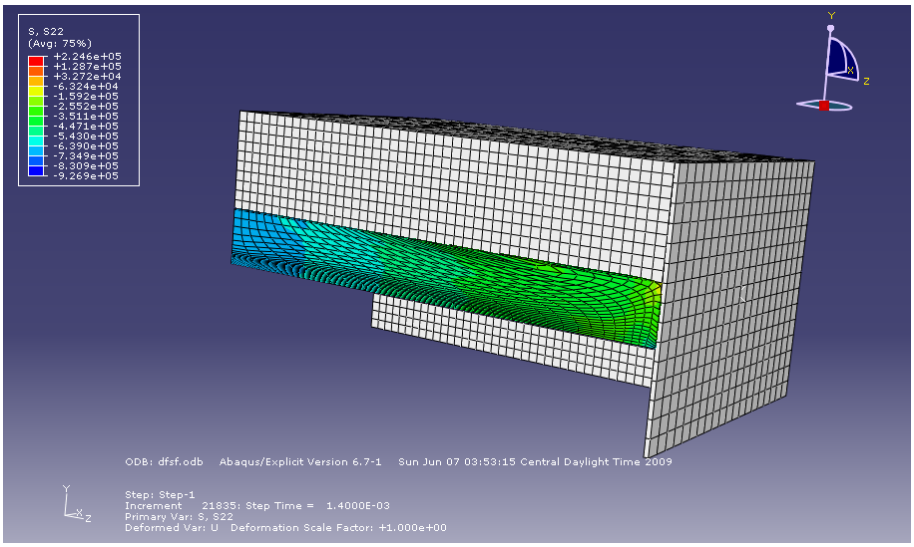

Figure 3.32 Deformed Shape at 1.1” Die Displacement (Abaqus)

Again, the results obtained from the simulation showed a close match to those obtained from the original 3-D simulation using MSC/Dyna.

Table 3.3 Die Displacement & Force (Abaqus)

Die Displacement (IN)	Force (LB) (Thousands)
0.3	-145
0.5	-135
0.7	-140
0.9	-137
1.1	-480

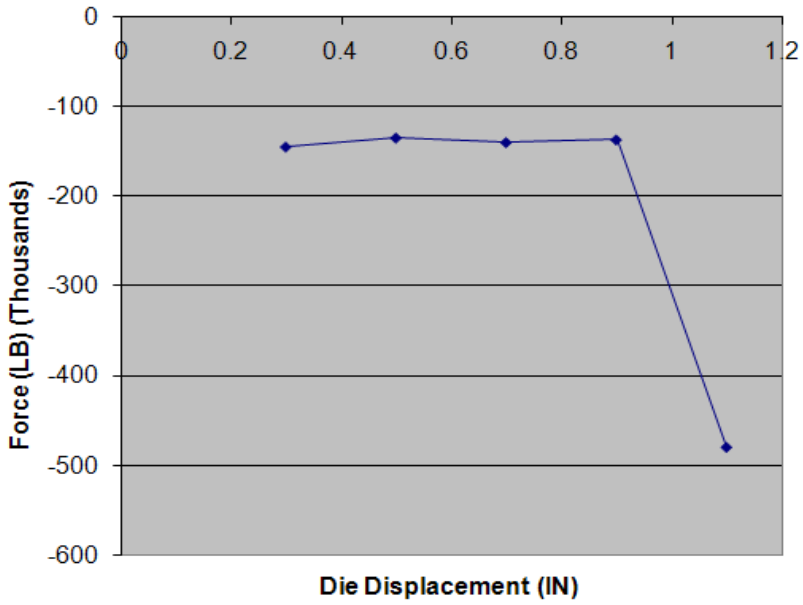

Figure 3.23 Force vs. Displacement (Abaqus)

The results of the above test problems demonstrated the validity of Ansys LSDyna and Abaqus in plasticity and set them up perfectly for an actual production forging problem.

CHAPTER 4

THE FORGING OF A MAN-WAY COVER

4.1 Forging of a Man-way Cover

As mentioned earlier, the process analyzed was that of an actual industrial production forging. It involved simultaneous heat transfer and stress-displacement phenomena and thus a fully coupled thermal-stress displacement analysis was required to be performed in both the software packages.

The circular billet was in contact with the ring and the base dies at the top and bottom surfaces and with the plunger at its center on the top surface. As the plunger moved vertically downwards, stresses were induced in the billet and heat transfer between the billet and the dies took place. Heat was also lost to the surrounding due to convection and radiation. The initial and final temperatures of the billet found out by experiments were 1425^{o}F and 1200^{o}F respectively. Figure 4.1 shows the stress-strain curves for a forging process.

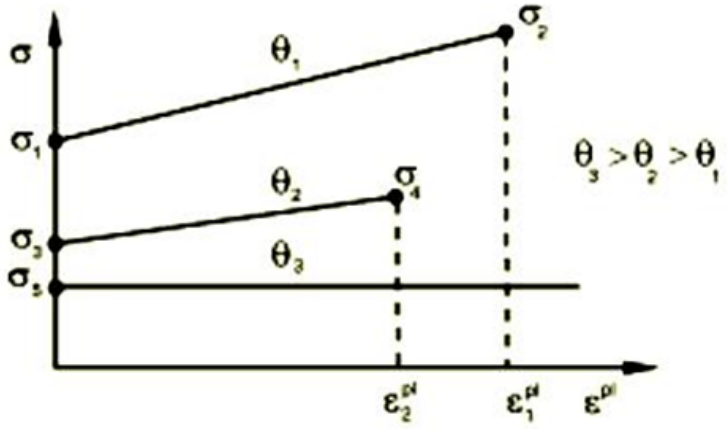

Figure 4.1 Stress vs. Plastic Strain [15]

As the temperature increases, the yield strength decreases. When the temperature becomes equal to or greater than the annealing temperature, the material is said to be in perfect plasticity as shown.

4.2 Material Properties

The billet material was ASME SA 516 Grade 70. The material properties were difficult to obtain and so, the high temperature material properties of AISI 1025 carbon steel were used owing to its resemblance in chemical composition with SA 516. The material properties are specified below.

Table 4.1 Temperature, Yield Strength & Ultimate Tensile Strength

Temperature (^{0}F)	Yield Strength (psi)	Ultimate Tensile Strength (psi)
400	27000	61500
600	24000	57750
800	21000	55500
1000	19500	52500
1200	17500	43500
1400	15000	25500
1600	13500	18000

Table 4.2 Temperature, Young's Modulus & Poisson's Ratio

Temperature (^{0}F)	Young's Modulus (psi)	Poisson's Ratio
400	28000000	0.33
600	27000000	0.33
800	25000000	0.33
1000	22000000	0.33
1200	16125000	0.33
1400	10375000	0.33
1600	7000000	0.33

Density (ρ) = 0.284 lb/in^3

The dies material was H-26. The material properties of H-26 are specified below:

Density (ρ) = 0.318 lb/in^3

Young's Modulus (Y) = 25000000 psi

Poisson's ratio (υ) = 0.33

4.3 Ansys LSDyna Simulation

In Ansys LSDyna, the forging process can be simulated in two ways: 1. Implicit to Explicit Sequential Solution 2. Time-varying Temperature Method [16].

The implicit to explicit sequential solution allows for the application of temperatures calculated in an Ansys thermal analysis as non-uniform loads in an explicit dynamic analysis. Temperature from any one specified time point in the thermal analysis can be applied in the explicit phase. The temperatures in the explicit phase do not vary with respect to time.

The second method uses EDLOAD command which can be used to apply a time-varying temperature to a nodal component.

Ansys LSDyna does not have the capability to simulate heat transfer phenomena like convection, conduction and radiation.

The time-varying temperature loading method was used to simulate the forging process since large amount of heat loss was observed in the process.

Owing to the nature of the problem, an axisymmetric model was considered as shown in Figure 4.2.

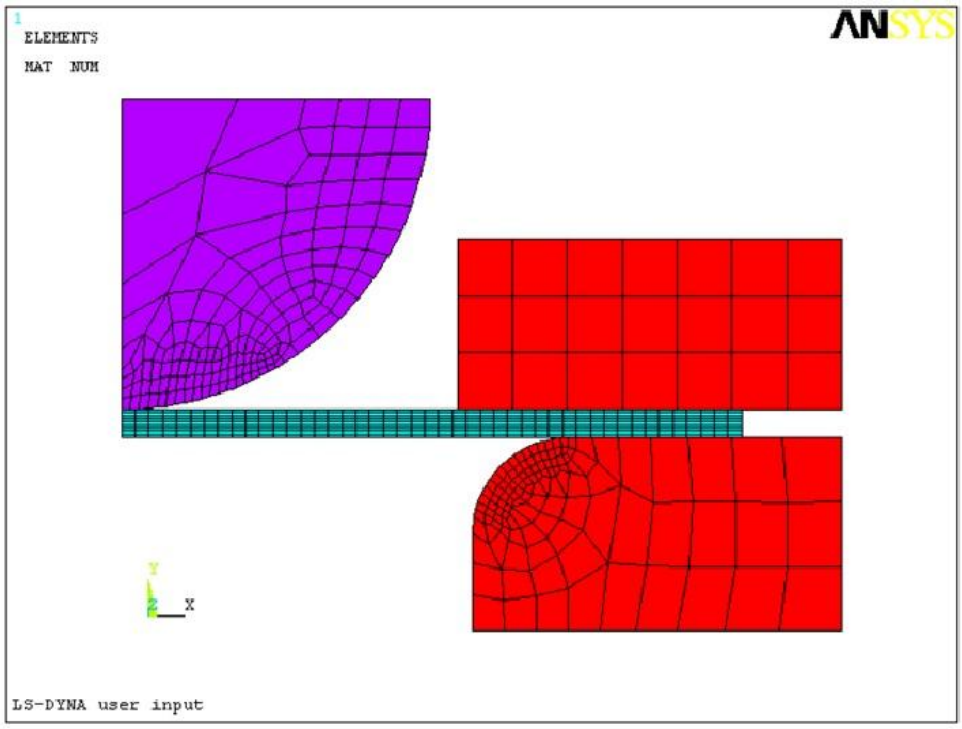

Figure 4.2 Axisymmetric Model (Ansys LSDyna)

A non-linear inelastic temperature dependent bilinear isotropic material model was defined for the billet. In this model, the stress-strain behavior at up to only six different temperatures can be specified. The plunger and the dies were defined rigid by the rigid body material model. The billet, plunger and the dies were meshed with Plane162 4node elements. The billet consisted of 405 elements. It was constrained at the axis of symmetry from moving in the X (horizontal) direction as shown. The plunger was constrained to move only in the Y direction whereas, the ring die and the base die were fixed at their respective positions.

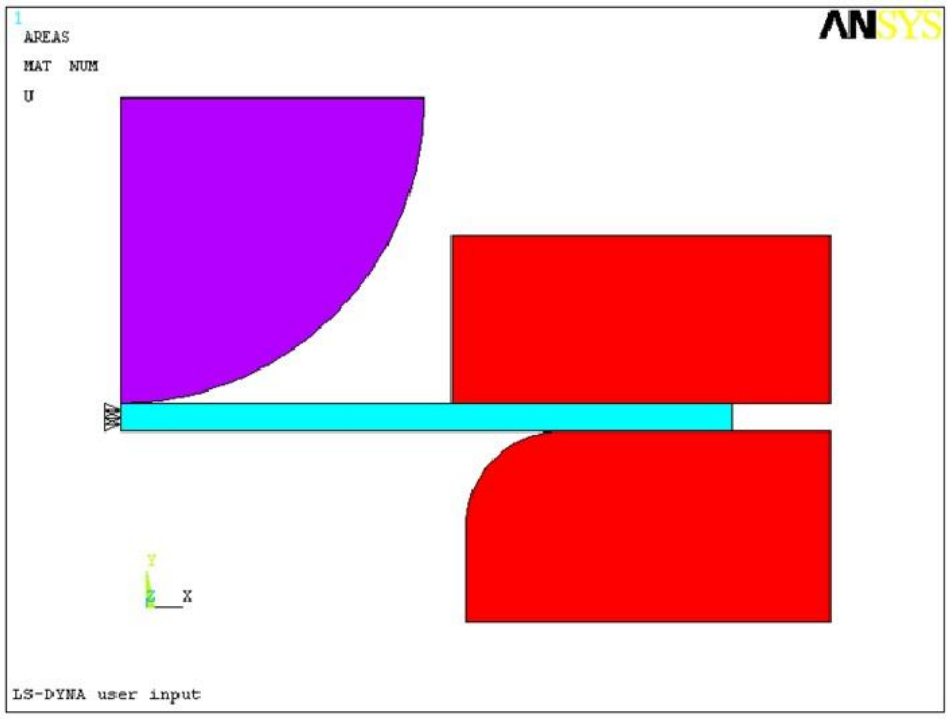

Figure 4.3 Boundary conditions

The plunger was displaced vertically downwards using the EDLOAD command and the time and displacement values were defined by using the array parameters. The analysis was carried out for 19.5 seconds.

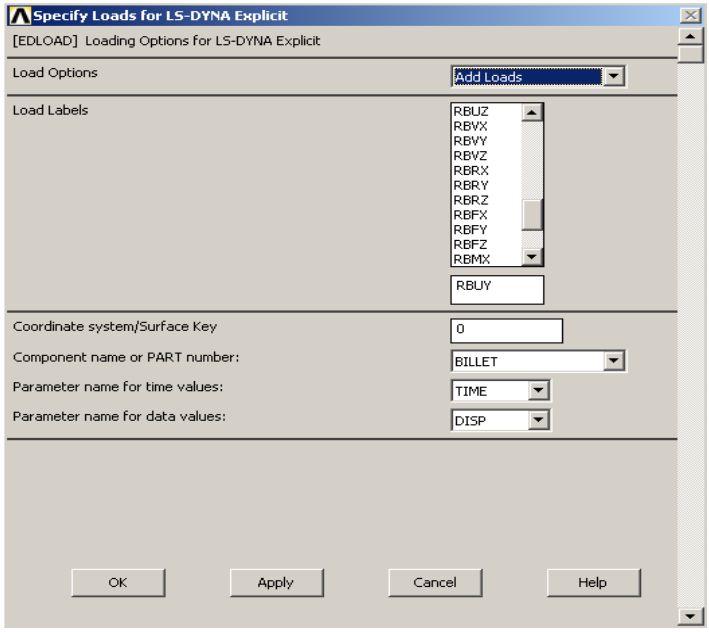

Figure 4.4 The EDLOAD command

The displacement data for the analysis was provided by reference 5 and is shown below.

Table 4.4 Displacement Values from 1-19.5 seconds

Time (sec)	Displacement (in.)
1	-0.8
2	-1.8
3	-2.8
4	-3.8
5	-4.5
6	-4.9
7	-5.5
8	-5.8
9	-6.1
10	-6.7
11	-7.0
12	-7.4
13	-7.9
14	-8.3
15	-8.6
16	-8.9
17	-9.3
18	-9.8
19	-10.3
19.5	-10.75

4.3.1 Ansys LSDyna results

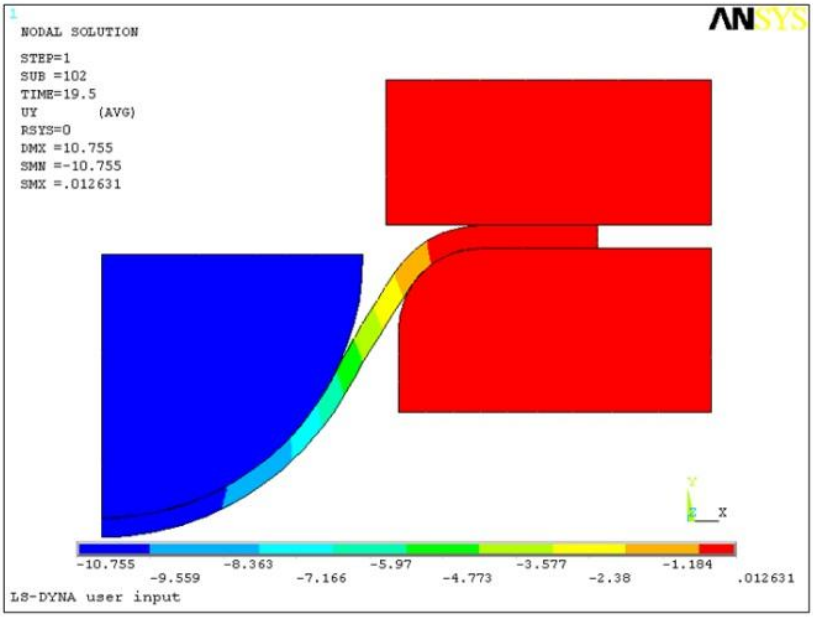

Figure 4.5 Deformed Shape - Axisymmetry (Ansys LSDyna)

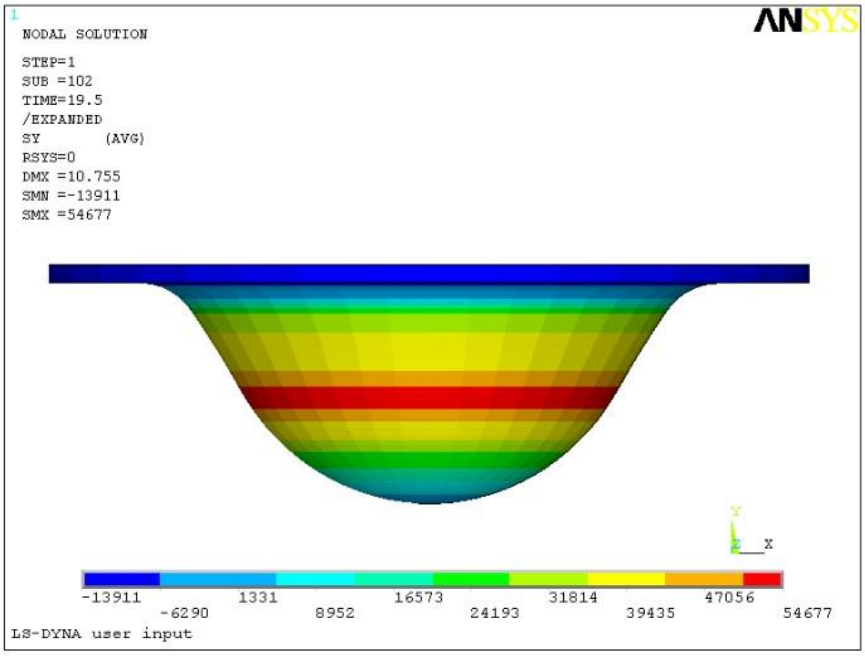

Figure 4.6 Deformed Shape - revolved 360^0 (Ansys LSDyna)

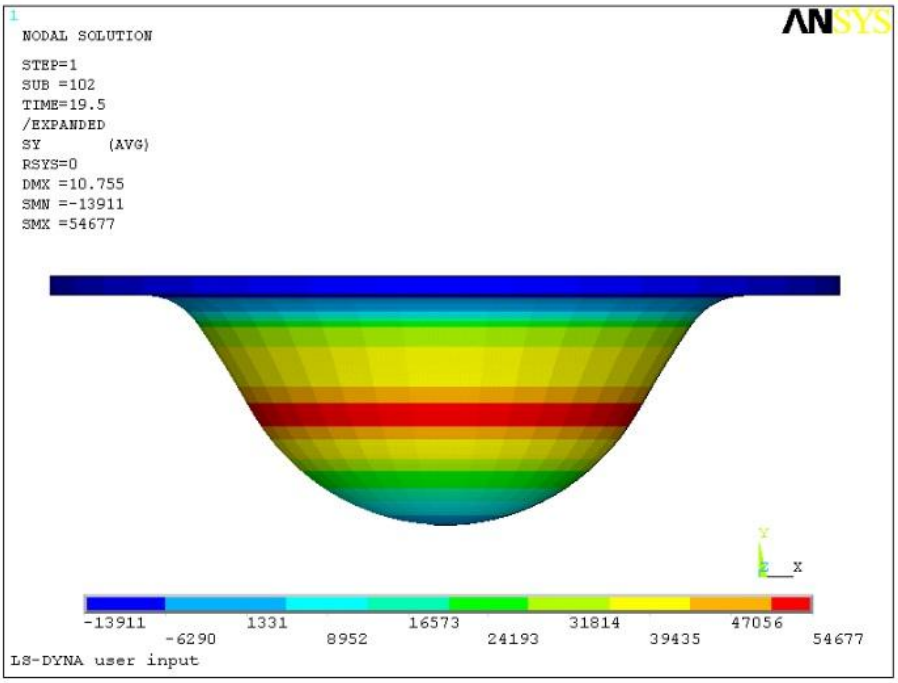

Figure 4.7 Stress Distribution (Ansys LSDyna)

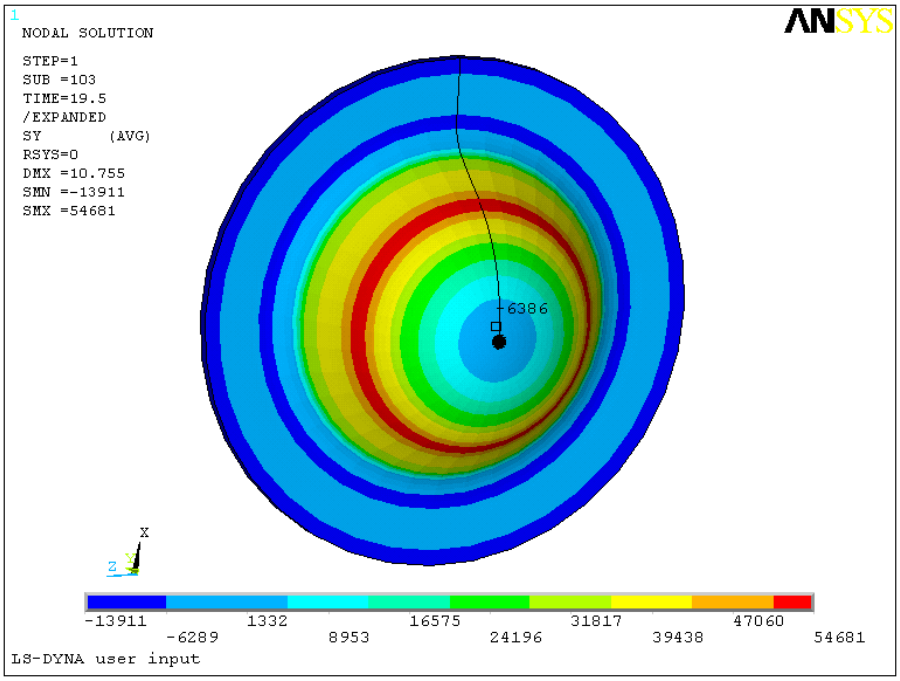

Figure 4.8 Stress at the Center of the Billet

From the query result option in Ansys LSDyna, it can be seen that the stresses generated at the center of the billet in the Y direction were found to be around of -6386 psi. The results obtained from Ansys LSDyna were in agreement with those obtained from reference 5.

4.4 Abaqus Simulation

A similar axisymmetric model was used in Abaqus. The billet was constrained to move across the plane of symmetry by applying the X-directional symmetric boundary conditions. The plunger and the dies were defined as rigid using the rigid body constraints. Constraints were applied on the reference points defined on the rigid bodies. The plunger was constrained to move only in the Y direction. The ring die and the base die were kept fixed.

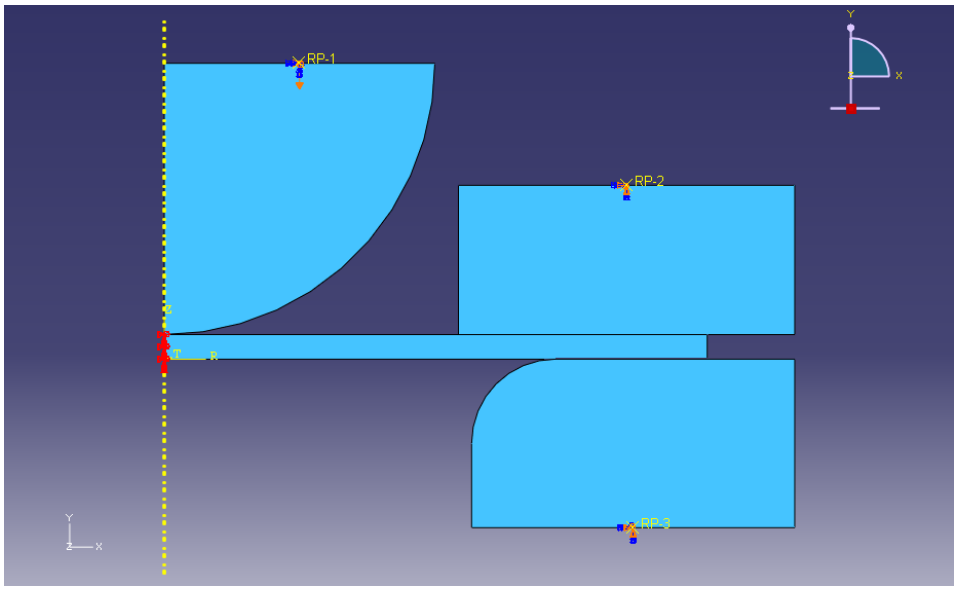

Figure 4.9 Axisymmetric Model (Abaqus)

The model was meshed with CAX4RT (Continuum axisymmetric 4 node reduced integration, bilinear displacement-temperature) element. The billet consisted of 390 elements. A dynamic explicit step was defined for the analysis. Temperature and displacement loads were defined to the billet and the plunger respectively by using the boundary condition option fused with the amplitude table.

Table 4.4 Temperature

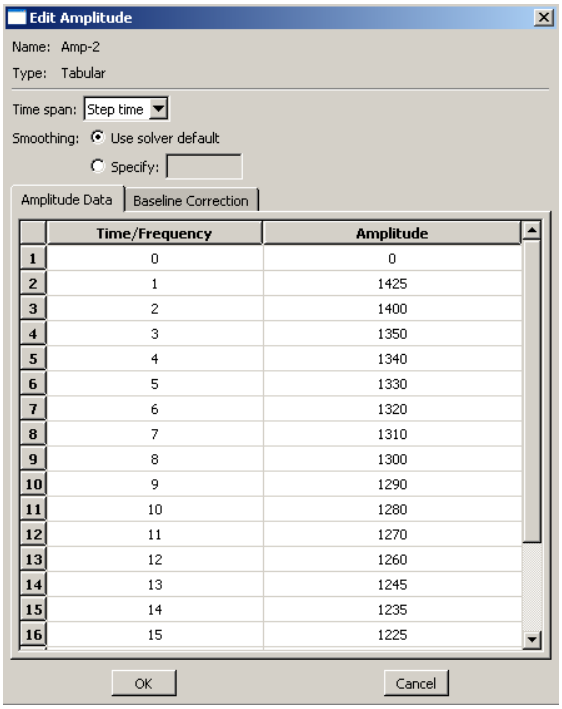

Table 4.5 Displacement

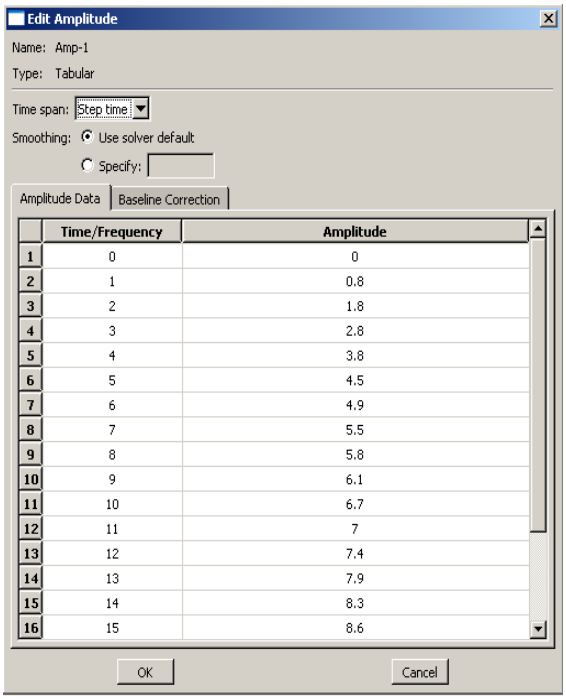

The analysis was run for 19.5 seconds with the total Y-directional deformation to be 10.5 in. The results of the analysis are shown below.

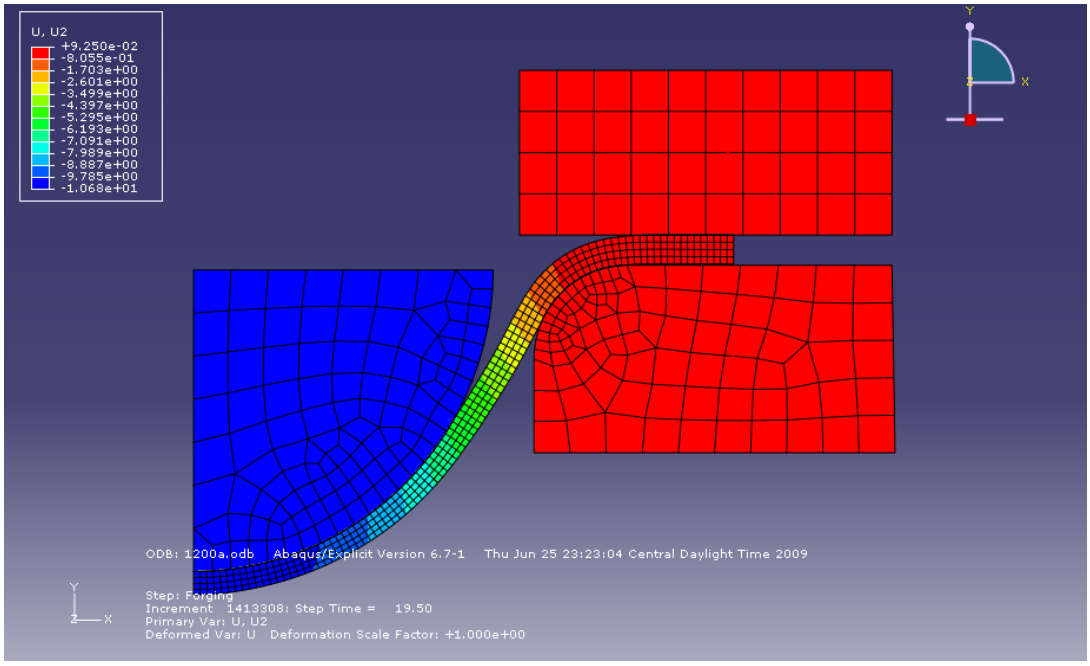

Figure 4.10 Deformed Shape (Abaqus)

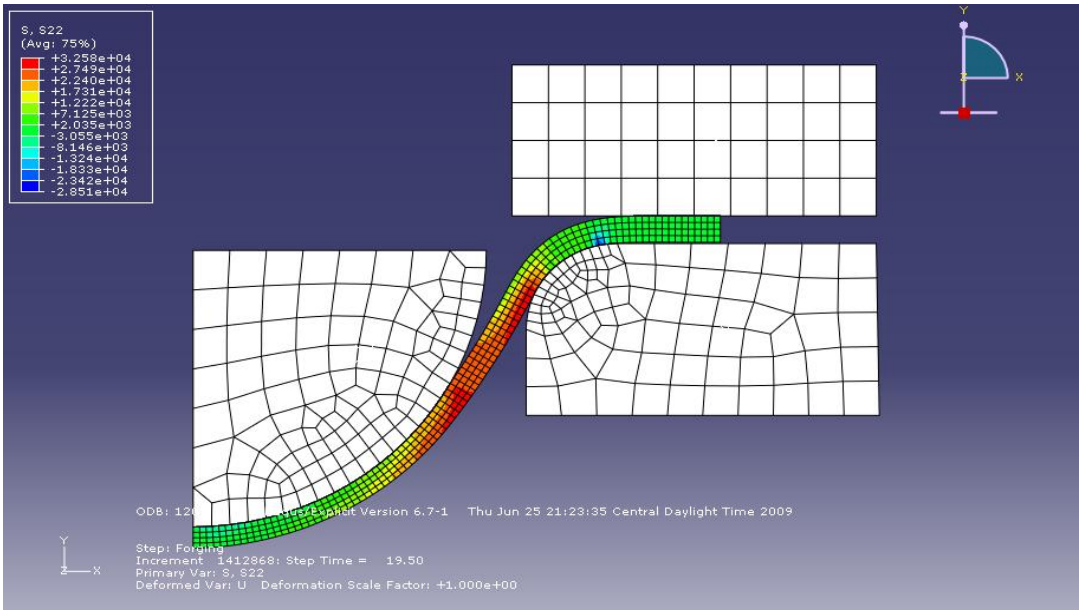

Figure 4.11 Stress distribution (Abaqus)

4.4.1 Abaqus Results

At the end of the simulation, a compressive stress of -6228 psi was observed at the center of the billet. The Abaqus results were in good agreement with those obtained from reference 5.

4.5 Final Results

The simulation results of Ansys LSDyna and Abaqus are shown below along with the results from reference 5.

Table 4.6 Final Results

	Private Communication (ARRI*), FORGE 3D	Private Communication (ARRI*), Experiment	Ansys LSDyna	Abaqus
Compressive Stress (Y-direction) (psi)	-5818	-6189	-6386	-6228

***** Automation and Robotics Research Institute

Ansys LSDyna showed a slightly higher stress value of -6386 psi at the center of the billet at full deformation while Abaqus showed a value of -6228 psi. The stress results obtained from Abaqus was in good agreement with the data provided by reference 5.

CHAPTER 5

CONCLUSIONS AND RECOMMENDATIONS

In this paper the effectiveness of general package software like Ansys LSDyna and Abaqus was tested in the process of forging. Ansys LSDyna and Abaqus, both, performed well for simple plasticity problems involving no heat transfer. So as to get a good insight into their abilities a simultaneous temperature-displacement process was analyzed in both the software.

Ansys LSDyna showed slightly higher stress results for the simultaneous temperature-displacement problem. This behavior can be accounted by the fact that only six stress-strain curves could be defined for six respective temperature states. This imposed restrictions on the flexibility of the analysis being carried out. Morever, Ansys LSDyna does not have the capability to remesh adaptively which can be a very important factor in analyses involving large deformations.

Abaqus on the other hand had full control over the stress-strain data definition for a wide range of temperatures and these data could be easily incorporated in the analysis. Unlike Ansys LSDyna, heat transfer phenomena like thermal contact conductance, convection and radiation could be efficiently modeled in Abaqus making it a reasonable tool for simulating a simultaneous temperature-displacement process. Abaqus also had the ability of adaptive remeshing, making it a more robust and powerful tool than Ansys LSDyna.

Between the two, Abaqus can have an optimum utilization in multi-solution providing industries and thus, it can be considered as a potential candidate for replacing forming specific software packages at a cheap cost.

REFERENCES

[1] Queen City Forging Co. (www.qcforge.net).

[2] Duggirala R. and Badawy A., "Finite element method approach to forging process design", Journal of Materials Shaping Technology, Volume 6, Number 2 / June, 1988**.**

[3] (http://www.ansys.com/products/explicit-dynamics/ls-dyna/default.asp).

[4] (http://en.wikipedia.org/wiki/Abaqus).

[5] Private Communication.

[6] Ghaei A. and Movaheddy M. Die Design for Radial Forging Process using 3D FEM .Journal of Materials Processing Technology. 2006.

[7] Lu H., Wu C. and Xu J. Forging and Extrusion Analysis with LS-DYNA using 3D adaptive EFG Method.10th International LS-DYNA Users Conference.

[8] Zhang Z., Dai G., Wu S., Dong L., and Liu L. Simulation of 42CrMo steel billet upsetting and its defects analyses during forming process based on the software DEFORM-3D. Materials Science and Engineering. 2007.

[9] Wilson W., Schmid S., and Liu J. Advanced simulations for hot forging: heat transfer model for use with finite element method. Journal of Materials Processing Technology, 2004.

[10] Bang W., Lee C. and Chang Y. Finite Element Analysis of hot forging with flow softening by dynamic recrystallization. Journal of Materials Processing Technology. 2002.

[11]Chakrabarty J. Theory of Plasticity. Elsevier Butterworth-Heinemann, 2006.

[12] Altan T., Ngaile G, Shen G. Cold and hot forging applications and fundamentals. ASM International. 2006.

[13] Seely B. F. & Smith O. J. Advanced mechanics of materials. John Wiley & Sons, Inc. 1959.

[14] Schleider W. M. Three Dimensional Simulation of Closed Die Forging Process Using MSC/ DYNA. Mercer University Engineering Research Center, 1994.

[15] Abaqus Manual.

[16] Ansys LSDyna Manual.